Effect of adhesion and tribological properties of modified composite nanostructured multi-layer nitride coatings on WC-Co tools life.

Alexey Vereschaka[1], Sergey Grigoriev[1], Anatoliy Aksenenko[1], Nikolay Sitnikov[2], Andre Batako[3], Mars Migranov[5], Svetlana Shevchenko[1] and Nikolay Andreev[5]

[1]Moscow State Technological University STANKIN, Vadkovsky per. 1, Moscow, 127994, Russia

[2]National Research Nuclear University MEPhI (Moscow Engineering Physics Institute), Kashirskoeshosse 31, Moscow, 115409, Russia

[3]Liverpool John Moores University (LJMU), Liverpool, UK

[4]Ufa State Aviation Technical University, March St., Ufa, Russia

[5]National University of Science and Technology "MISiS", Leninsky prospect 4, Moscow 119049, Russia.

Abstract:

The paper presents the results of the comparative tests of carbide samples with multilayered nano-structured coatings based on titanium nitrides (Ti-TiN-(Ti,Cr,Al,Si)N) and zirconium nitrides (Zr-ZrN-(Nb,Zr,Cr,Al)N and Zr-ZrN-(Zr,Al,Si)N). The phase composition and microstructure of these coatings were studied. The scratch test method was applied to study the adhesion bond strength to the substrate and the coating fracture patterns. The tribological parameters of the coated samples were studied at temperatures of 450°C-900 °C. The cutting properties of the tools with the coatings under study were investigated in turning AISI 321 steel. Various coating parameter effects on the cutting tool life were studied.

Keywords: PVD coatings; coefficient of friction; tool life; thermo stability

1. INTRODUCTION

Modification of surface layer of metal-cutting tools through deposition of modifying coatings is an important resource for improving their performance properties (tool life, reliability, ability to work at elevated cutting speeds and feeds, thermo stability, etc.). In turn, the challenge to evaluate coating properties and identify key factors affecting the working efficiency of coated tools is a very complex and not completely solved task. High temperature in the cutting zone (up to 1000-1100°C) is an important factor (and sometimes a key factor) affecting the performance properties of metal-cutting tools. Therefore, thermal stability, including resistance to oxidation at high temperatures, is an important requirement for modern modifying coatings of metal-cutting tools.

The thermal stability of TiN and CrN coatings is about to 550 and 600 °C [1], respectively. CrN oxidizes to Cr_2O_3 and nitrogen is released, without being bound to the growing Cr_2O_3 scale. TiN forms a layered TiO_2 scale and nitrogen has a tendency to escape during oxidation [2]. ZrN system is sufficiently stable at temperatures not exceeding 850 °C, but at higher temperatures, grains start to grow and that leads to a significant decrease in hardness [3]. When temperature is raised up to 550 °C, the process of active oxidation starts, during which tetragonal t-ZrO_2 are formed, and at temperatures exceeding 950 °C, monoclinic (m-ZrO_2) are formed [4]. (Zr,Al)N system maintains its stable hardness up to temperature of 1100 °C [3]. (Ti,Al)N and (Ti,Cr)N

coatings show the stability up to 750 °C [5]. (Ti,Zr)N and (Ti,Ta)N systems remain thermally stable at temperatures up to 850 °C[6]. NbN system remains stable at temperatures up to 700 °C [7]. For this coating, the growth mechanism of the Nb_2O_5 scales was dominated by an inward diffusion of oxygen through the oxide scales. The active oxidation of the above coating begins at temperature of 450 °C [8].

(Ti,Cr)N has been attracting more attention owing to high hardness (4000 HV), high temperature oxidation resistance (600°C), and low friction coefficient (0.3) [9,10]

Thermal annealing of $Cr_{1-x}Al_xN$ coatings up to 900 °C induces a transformation towards their stable phases of wurtzite (w-) AlN, and then cubic (bcc-) Cr via intermediate phase of hexagonal (h-) Cr_2N with concomitant N-loss, and thereby causes a deterioration of the mechanical properties [11]. Compared with TiN and (Ti,Al)N coating, (Ti,Al,Cr)N coating gets more attention due to its higher hot hardness and oxidation resistance [12,13]

M. Danek [14] reported that the increase of Cr contents in TiAlCrN coating could significantly enhance the oxidation resistance.In order to avoid brittle failure due to cracking, wear-resistant coatings must be both hard and tough. Based on these criteria, Ou et al. [15] reported in a first principles study of the elastic properties of $Ti_{1-x}TM_xN$ alloys (TM = Y, Zr, Nb, Hf, and Ta) that TiN highly alloyed with NbN or TaN exhibits significantly improved ductility. TiAlN-based quaternaries were shown to exhibit significant increases (up to 23%) in bulk moduli B accompanied by progressive decreases (up to 45%) in elastic stiffness E and shear resistances G and C_{44} for rising concentrations of V, Nb, Ta, Mo and W. Deeper insights indicated the electronic origin of toughness enhancements in cubic TiAlN based systems to be related with the valence electron configuration, as seen for ternary alloys [16].

Incorporation of elements providing increased d-electron concentrations (e.g. Nb, Ta, Mo, and W), significantly changes the electronic structure of TiAlN, which evolves from exhibiting occupied anti-bonding metal-metal states into highly bonding metallic states, whilepreserving strong metal-N bonding [17]. It has been shown that the thermal stability and hardness can be improved by alloying Ti1-xAlxN with an additional transition metal (Me). For example, $Ti_{1-x-y}Al_x(Cr)_yN$ has shown enhanced hardness after annealing above 1000 ºC [18,19]. Experimentally, the fracture toughness of $Ti_{1-x-y}Al_x(Nb)_yN$ has been found to enhance with the addition of Nb [20].At 1000 °C, h-AlN has formed for (Ti,Al,Cr)N, for (Ti,Al,Nb)N it forms only when annealed at 1100 °C [21]. At 1100 °C, Hardness drops to ~30 GPa for (Ti,Al,Cr)N and (Ti,Al,Nb)N while Hardness of TiAlN decreases to 27.7 ± 0.8 GPa [21]. The critical load (L_c) for recovery spallation during scratching at 900 °C is maximum (118 ± 3) for (Ti,Al,Nb)N, and the parameter hardly changes in comparison with room temperature (120 ± 5), while for TiAlN, there is a significant decrease (from 114 ± 11 at room temperature down to 75 ± 4 at 900 °C) [21]. Thus, the coatings based on nitrides (in particular, TiN, CrN, ZrN, NbN) show rather low thermal stability and resistance to oxidation. With additional elements introduced in coating compositions, the above parameters can be increased significantly.

Another important factor, which predetermines the complication of the elemental compositions of coatings is in the fact that introduction of additional elements makes it possible to restrain the growth of grains. In particular, adding Al to the ZrN films decreases the grain size drastically and nanometer sized amorphous regions form. The decrease in grain size can be attributed to the low solubility of AlN in ZrN and to the high nitrogen content in the Al containing films [3]. The addition of silicon led to an increase in hardness of coatings. An increase in hardness was explained in the framework of a two-step mechanism, i.e., by forming a solid solution of Si atoms in NbN [22], TiN [22], ZrN [4], CrN [23], (Ti,Al)N [24], (Zr,Al)N [25], (Cr,Al)N [26], (Ti,Zr)N [27], (Ti,Cr)N [28], (Cr,Ti,Al)N [28], lattice and by forming a nanocomposite material. Addition of Si can also decrease penetrating of reactive agents into the coatings through the refine effect [29]. The incorporation of hard nanocrystalline TiAlN phases with

improved oxidation resistance, and Si_3N_4 amorphous phase achieving superhardness, has allowed increasing the hardness as well as thermal stability [3,4]
Other option for both improvement of mechanical characteristics and increase in a resistance to high-temperature oxidation is the formation of multilayered coating structures [4,20,30].
The properties of multilayered nano-structured coatings Ti-TiN-(TiCrAl)N, Zr-(Zr,Cr)N-CrN, Ti-TiN-(Ti,Cr,Al)N, Ti-(AlCr)N-(TiAl)N, Ti-(AlCr)N-(TiCrAl)N, Zr-(AlCr)N-(ZrCrAl)N, Ti-TiN-(TiCrAl)N, Zr-ZrN-(ZrNbCrAl)N are investigated in [32-42].

The most important mechanical characteristics of coatings affecting their performance characteristics are usually as follows:
- microhardness (affecting tool life of a coated tool);
- strength of adhesion bonds in the "coating-substrate" system;
- impact toughness (affecting crack resistance of coating)
- coefficient of friction.
The most important characteristic of coatings is also their thermo stability, that is, the ability of coatings to remain operative at the highest possible temperatures. Recently, special attention has been paid to the study of the properties of coatings at temperatures corresponding to the actual temperatures in the cutting zone [43, 44], since all of the above coating characteristics vary significantly at the above temperatures and often drastically differ from the values measured at room temperature. There are a number of studies aimed to determine the coefficient of friction in samples with different coatings, including at elevated temperatures.
Nohava et al [45] consider the properties of coatings (Al,Cr)N, α-$(Al,Cr)_2O_3$ and (Al,Cr)(O,N) in comparison with the properties of "reference" coating TiN-(Al,Ti)N. Meanwhile, the coatings under the study had three-layer structures, including adhesion layer – TiN, intermediate layer – nano-composite (Al,Ti)N, (Al,Ti)N-SiN_x, and an outer wear-resistant layer of the composition described above. The tribological tests were carried out at temperatures of 24, 600 and 800°C. The maximum value of the coefficient of friction (COF) was observed at temperature 600°C for all the studied samples, and at temperature 800°C, the study found out a significant decrease in the COF (down to 0.6-0.8), to the values lower than the one observed at room temperature (0.3-0.5). Bao et al [46] studied the properties of multilayered CVD coating Ti(C,N)-TiC-TiN. The COF was measured at room temperature and at temperature 550°C and reached 0.4-0.5 and 0.6-0.7, respectively.
Therefore, it can be argued that:
- COF for samples with coatings changes significantly with an increase in temperature;
- this change is characterized first by the smooth growth of the COF with an increase in temperature, and then by a sharper decrease in the COF with a further increase in temperature.

2. EXPERIMENTAL

A complex system formed in the zones of actual contact of friction bodies has specific properties that differ from the properties of the materials of those bodies, considered outside friction contact. It is necessary to assess directly the properties of the contact zone, which can correlate with the main factors of friction and wear. The use for this purpose of contact forces, measured directly in friction of actual parts in conditions of elevated temperatures, is difficult for a number of reasons. Among them the particularly important reasons are as follows: uneven distribution of forces and temperature in the contact area, different chemical purity and resolution of contacting surfaces, which complicates the determination of actual contact loads.
The experimental method [47] was used to evaluate the tribotechnical parameters (τ_n, P_n,τ_n/P_n). The above method is based on a physical model (Fig. 1), which in the first approximation reflects the actual conditions of friction and wear on local contact. According to this model, a

spherical indenter 2 of the tool material (simulating individual roughness of a contact surface of solid bodies in friction) compressed by two plane-parallel samples 1 of the material being machined (with high precision and cleanliness of contacting surfaces) spins under load. The force F_{exp} to rotate the indenter and applied to cable 3 laid in a groove of disc 4 is mainly related to the shear strength τ_n of adhesion bonds. Since the measurements are made at elevated temperatures, thermal pads 6 made of material with low thermal conductivity are used. Electric current is supplied to copper plates 5 through regulating and power transformers. The current is selected depending on the required contact temperature.

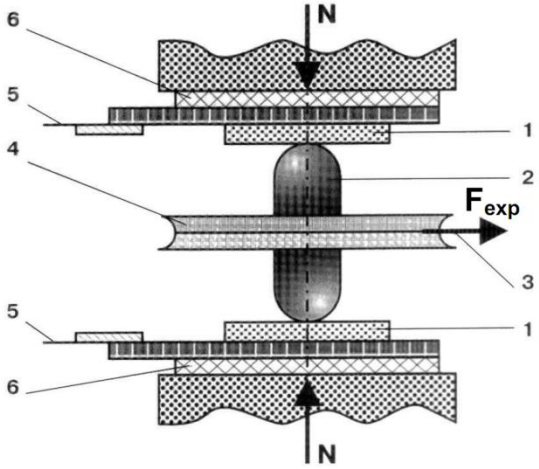

Fig. 1.Model of friction contact [47].

The strengthτ_n of adhesion bonds on cut is determined from the relation:

$$\tau_n = \frac{3}{4} \cdot \frac{F_{exp}}{\pi} \cdot \frac{R_{exp}}{r_{ind}^3} \tag{1}$$

where F_{exp} – the circumferential force on the disk, rotating the indenter;
R_{exp} – the radius of the disk in which the indenter is fixed;
r_{ind} – the radius of the indent on the samples.

Because of the small dimension of the indent, it is assumed that the normal stresses acting on the surface of the sphere are constant and equal in the area of the entire indent. They are defined as follows:

$$p_n = \frac{N}{n \cdot r_{ind}^2} \tag{2}$$

The adhesion (molecular) component of the coefficient of friction (COF) is as follows:

$$f_M = \frac{\tau_n}{p_n} = \frac{3}{4} \cdot \frac{F_{exp}}{N} \cdot \frac{R_{exp}}{r_{ind}} \tag{3}$$

In order to use the method discussed above in the conditions of elevated temperatures of contact, special equipment (adhesiometer) has been developed [48] to heat the contact zone and provide a characteristic temperature distribution over the depth of the contacting bodies.

Two-sided spherical cylinders (with a radius of 2.5 mm and a height of 25 mm) made of tool materials (carbides) were used as indenter. The contact zone was subjected to heating after the installation of samples and an indenter and application of the load *N*, under the action of which the indenter with a sphere of radius r_1 intruded into the samples to some depth *h*. There is plastic contact, and external friction is observed [47] in rotation of a cutting punch.The assumed loads and low roughness of the contacting surfaces provide not only the necessary area of the actual

contact between the samples and the indenter, but also the extrusion (rupture) of the formed films (oxide and sorbed ones) and the contact of relatively pure metal surfaces. That ensures a high density of contact between the indenter and the samples, and that almost excludes the penetration of air oxygen into a large part of the contact area. To ensure homogeneity of physico-mechanical properties, the samples are made from the same workpiece. The experiments are carried out at different values of the contact temperature θ. Thus, relations of $\tau_n = f(p_n)$ are obtained at different values of θ.

According to the studies carried out using the described method, the reliable data on value τ_n can be obtained at 2-3 repetitions of the experiment, while the probable deviation does not exceed 5 %.

Conditions of deposition: VIT-2 installation using filtered cathodic vacuum arc deposition (FCVAD) [32-42] technology. To study the effect of thickness of a separate nanolayer on mechanical and performance properties of a coating, a nanolayer with increased thickness (approximately 2, 4 and 9 times thicker than average thickness of a nanolayer) was created in composition of outer wear-resistant layer of the coating (approximately in the middle of the layer). [32-37] present justification for selection of composition for a multilayered coating.

X-ray diffraction analysis method was used to determine phase compositions of the samples. Diffraction patterns were obtained by X-ray diffractometer PANalyticalEmpyreanSeries 2 with monochromatized CuKα radiation. The patterns were got in asymmetric geometry with incidence angle of parallel (sliding) beam of ω=3÷5º.The phase composition analysis was performed with PANalyticalHighScorePlus and ICCDPDF-2 data base using the Feldman-and-Mayer technique [49].

A Nanovea Mechanical tester (Nanovea, USA) scratch tester was used to determine the adhesion/cohesion strength, scratch resistance, as well as to investigate mechanism of failure. A diamond conic indenter of Rockwell type with radius of curvature of R = 100 μm was used to apply scratches to a coating surface with a continuously increasing load from 0 up to 40 N and a loading rate of 10 N/min.

Conditions of cutting tests: lathe CU 500 MRD; turning material: steel AISI 321(see Tab. 1). Cutting tool: carbide inserts SNUN ISO 1832:2012 made of carbides (WC+6% Co); tool geometry: γ = –8°; α= 6°; K = 45°; λ = 0; R = 0.8 mm; cutting modes: f = 0.2 mm/rev; a_p = 0.5 mm; v_c = 300 m min^{-1}.

Table 1.Chemical composition of steel AISI 321.

C	Si	Mn	Ni	S	P	Cr	Cu
up to 0.12	up to 0.8	up to 2	9 - 11	up to 0.02	up to 0.035	17 - 19	up to 0.3

3. RESULTS AND DISCUSSION

Microstructure analysis

The microstructures of the coated samples under the study are shown in Fig. 2-4.

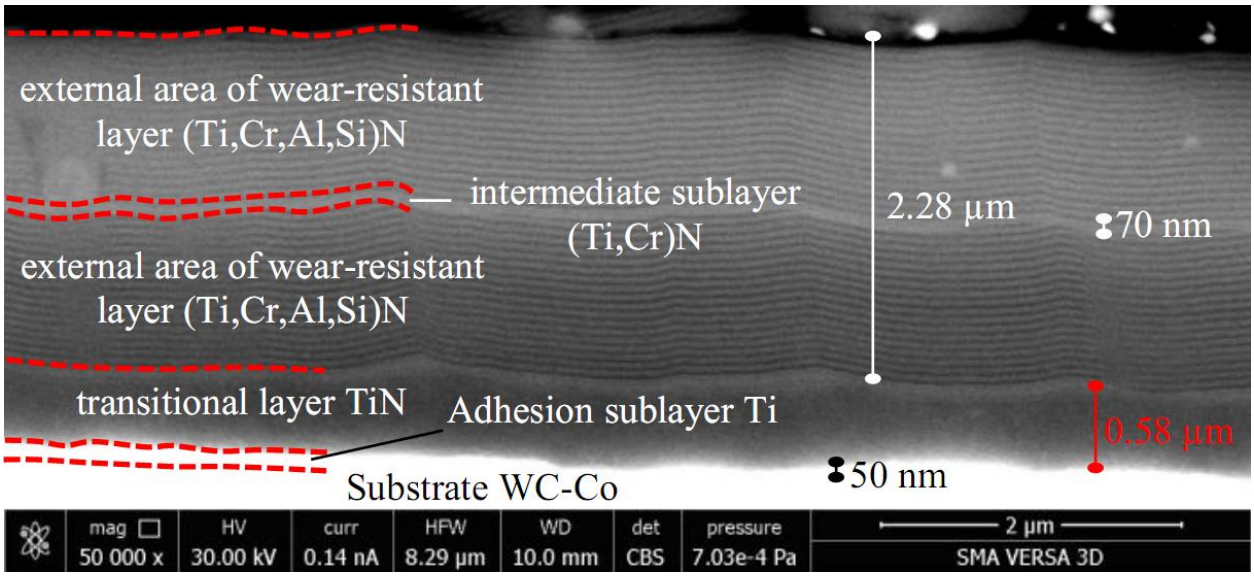

Fig. 2. Structure of coating Ti-TiN-(Ti,Cr,Al,Si)N.

The total thickness of coating Ti-TiN-(Ti,Cr,Al,Si)N is 2.98 µm. Wear-resistant layer (Ti,Cr,Al,Si)N has thickness of 2.28 µm and comprises 73 nanolayers with average thickness of about 30 nm, as well as intermediate sublayer (Ti,Cr)N with thickness of 70 nm. This sublayer, which is thicker than other nanolayers, is introduced to study the influence of the nanolayer thickness on the failure mode of the coating. Thickness of transitional layer TiN is 0.58 µm. Thickness of adhesion sublayer Ti is 50 nm.

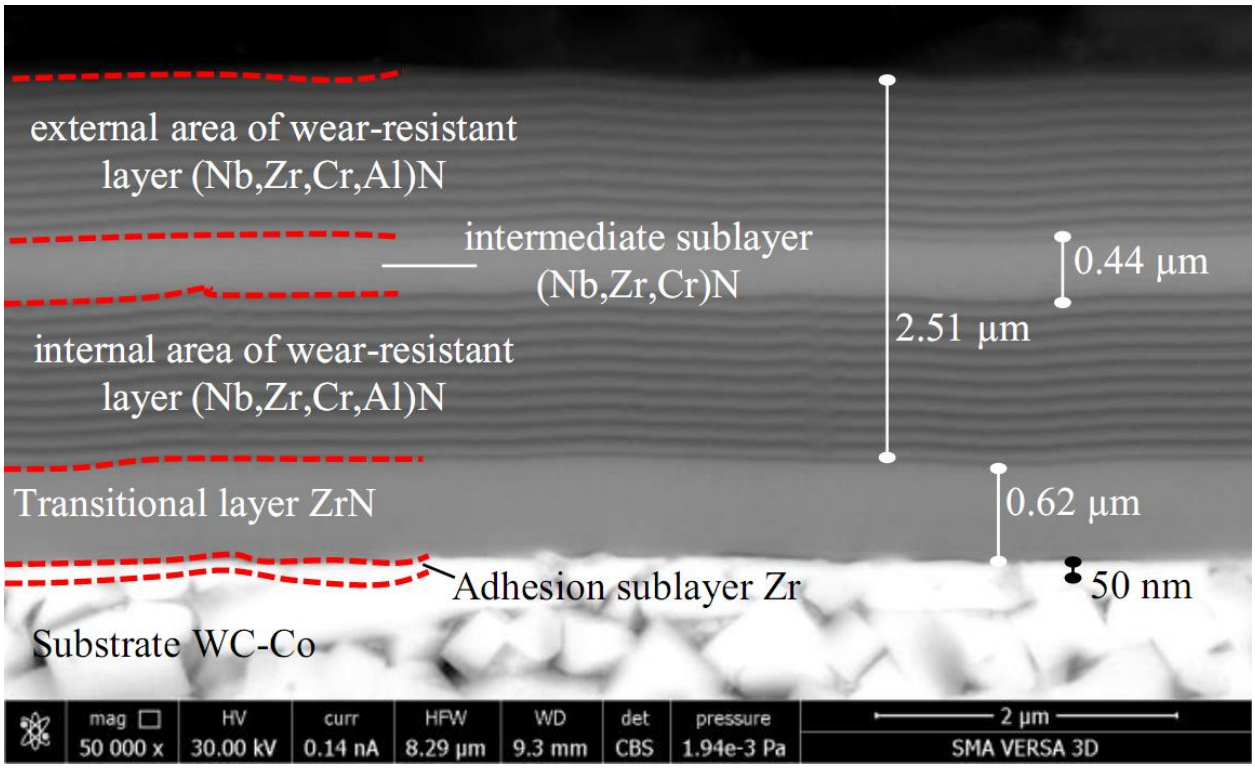

Fig. 3. Structure of coating Zr-ZrN-(Nb,Zr,Cr,Al)N.

The total thickness of coating Zr-ZrN-(Nb,Zr,Cr,Al)N is 3.13 μm. Wear-resistant layer (Nb,Zr,Cr,Al)N has thickness of 2.51 μm and comprises 41 nanolayers with average thickness of about 50 nm, as well as intermediate sublayer (Ti,Cr)N with thickness of 0.44 μm. This sublayer, which is thicker than other nanolayers, is introduced to study the influence of the nanolayer thickness on the failure mode of the coating. Thickness of transitional layer ZrN is 0.58 μm. Thickness of adhesion sublayer Zr is 30 nm.

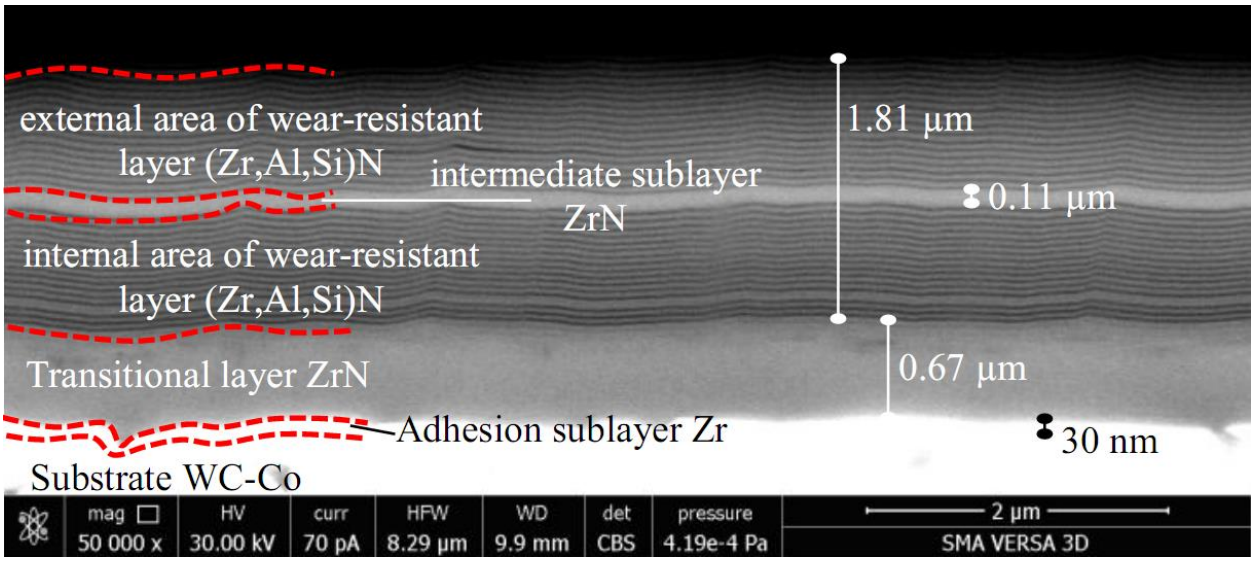

Fig. 4. Structure of coating Zr-ZrN-(Zr,Al,Si)N

The total thickness of coating Zr-ZrN-(Zr,Al,Si)N is 2.48 μm. Wear-resistant layer (Zr,Al,Si)N has thickness of 2.51 μm and comprises 67 nanolayers with average thickness of about 25 nm, as well as intermediate sublayer ZrN with thickness of 0.11 μm. This sublayer, which is thicker than other nanolayers, is introduced to study the influence of the nanolayer thickness on the failure mode of the coating. Thickness of transitional layer ZrN is 0.58 μm. Thickness of adhesion sublayer Zr is 30 nm.

Microhardness of coatings

The coatings under the study have the following microhardness (measured at room temperature):
coating Ti-TiN-(Ti,Cr,Al,Si)N– 36GPa
coating Zr-ZrN-(Nb,Zr,Cr,Al)N–26 GPa
coating Zr-ZrN-(Zr,Al,Si)N–28 GPa

Phase composition analysis

Sample with Ti-TiN-(Ti,Cr,Al,Si)N coating
When applying a coating, among the possible phases expected to form, there were as follows: α-Ti; cubic δ-TiN; $CrTiN_2$, Cr_2N, CrN, cubic AlN, TiAlN, CrAlN, Ti_3AlN,$Ti_2Al_2N_2$. Phases with Si were unlikely to form because of the low Si content both in the coating itself and in cathode Al-Si (Al90 at%, Si 10 at%) used to apply the coating. Meanwhile, even in small volumes (2-3 at%) Si produces a noticeable positive effect on the properties of the coating [45]. A diffraction pattern of Ti-TiN-(Ti,Cr,Al,Si)N coating is shown in Fig. 5. The coating includes

phases of α-Ti (space group P63/mmc, a=2,9500Å, c=4,6830 Å), TiN(a=4,2400 Å) andCrTiN2 (a=4,1850 Å) (space group Fm-3m). With high probability, the coating includes a phase of Cr_2N (space group P63/mmc, a=2,7600Å, c=4,460 Å). A phase of α-Ti is a part of a sublayer deposited on the substrate to increase the adhesion of the coating to the base. The absence in the composition of precipitated phases Al can indicate the possible dissolution of Al in nitrides Ti and Cr with formation of solid solutions on their base with a change in the parameters of the crystal lattice.

At elevated temperatures the metastable c-TiAlN phase decomposes into the equilibrium binary phases, c-TiN and h-AlN. The onset of transformation to h-AlN is leading to the decrease in hardness observed at annealing temperatures above ∼900 ◦C [50]. Lind et al. [51] showed that by alloying (Ti,Al)N with Cr, metastable (Cr,Al)N was formed during annealing as well as stable (Ti,Cr)N. The smaller free energy of the (Cr,Al)N phase compared to (Ti,Al,Cr)N and (Ti,Al)N makes the formation of this phase energetically favorable. In the (Zr,Al)N-TiN multilayers studied in [52] a similar result was found. There, intermixing at the multilayer interfaces during annealing caused formation of a metastable Zr(Ti,Al)N phase. The formation of this new phase and the simultaneous dissolution of Zr in the TiN sublayers decreases the lattice parameter mismatch between the phases. The TiZrN phase has a smaller miscibility gap than ZrAlN [53,54] why the formation of the new metastable phase is energetically favorable.

H.C. Barshilia et al. [55] showed that multilayer structure of Ti and Cr nitrides are characterized not only by enhanced mechanical properties, but also by higher thermal stability as compared to a single layered TiN and CrN coatings. Oxides begin to form at temperatures above 750°C. In multilayer coatings interdiffusion between the layers and different diffusion properties of O, N, Ti and Cr in TiN and CrN make the oxidation mechanism of Ti and Cr nitrides multilayers very complex.

Solid phases Cr_2N is more covalent than CrN and it exhibits a higher hardness. Also, Cr_2N layers have lower residual stresses than CrN, but CrN has better oxidation resistance than Cr_2N. So dual phases coatingsCr_2N+CrN enable to control the residual stresses of the films from tensile to compressive by different volume fraction of each phase [56].

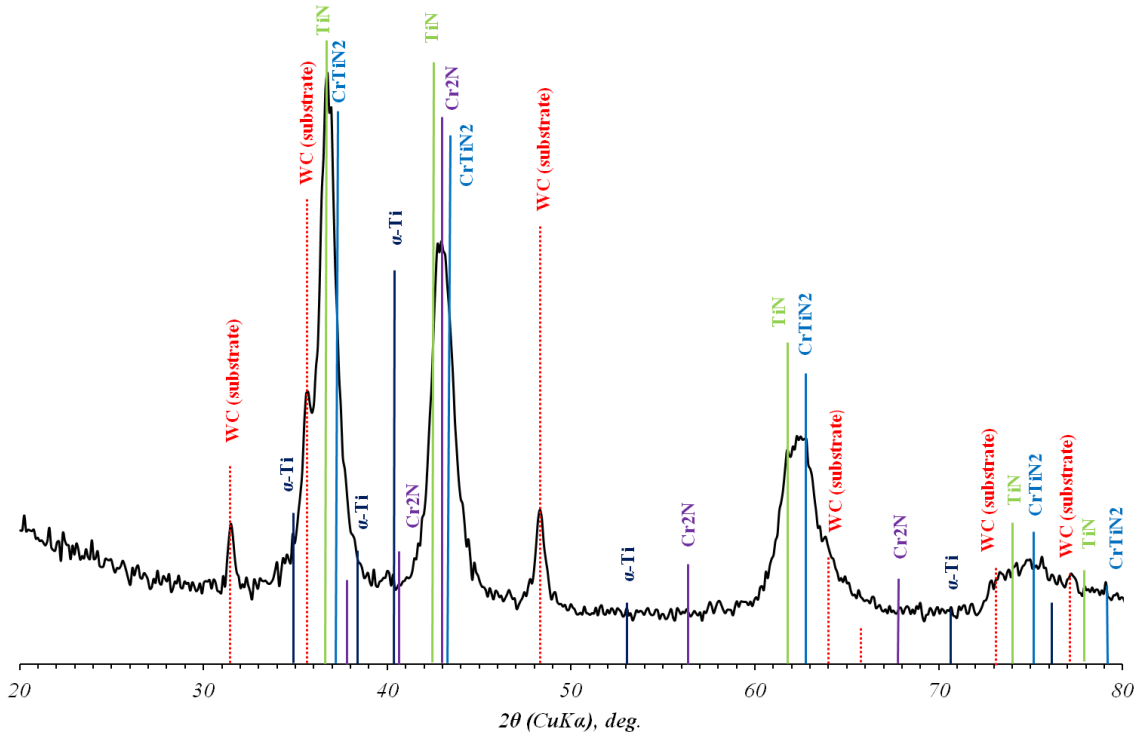

Fig. 5. XRD pattern of Ti-TiN-(Ti,Cr,Al,Si)N coating on WC-Co substrate

Sample with Zr-ZrN-(Nb,Zr,Cr,Al)N coating

The coating can theoretically include the following phases: Zr, cubic δ-ZrN; α-ZrN;Zr_2N;ZrAlN; Cr_2N, $NbZrN_2$; CrN; hexagonal β-Nb_2N; cubic δ-NbN; hexagonal ε-NbN; hexagonal δ'-NbN; hexagonal g-Nb_3N_4; tetragonal Nb_4N_3; cubic AlN; cubic (Zr,Nb)N; cubic NbAlN.

A diffraction pattern of Zr-ZrN-(Nb,Zr,Cr,Al)N coating is shown in Fig. 6. The coating includes phases of ZrN (space group Fm-3m, a=4,5978 Å), $NbZrN_2$ (space group Fm-3m, a=4,5000 Å) and CrN (space group Fm-3m, a=4,5978 Å). Considering the fact that individual reflexes of the phase Cr_2N are not found at XRD pattern, unambiguously estimate the presence or absence of this phase is not possible. No phases of Zr, ZrAlN, NbN etc. have been expressly detected, but it does not mean the coating does not include them. The coating certainly contains Zr sublayer, like in case of sublayer α-Ti in Ti-TiN-(Ti,Cr,Al,Si)N coating, but individual reflexes of Zr phase are not detected in XRD pattern due to its not enough intensity.

The formation of ZrAlN phase is the most probable. The cubic ZrAlN phase transforms by nucleation and growth of hexagonal AlN when annealed above 900 ◦C. Annealing of hexagonal ZrAlN thin films above 900 ◦C causes formation of AlN and ZrN rich domains within the hexagonal lattice. The cubic TiAlNbN quaternary solid solutions are metastable with respect to decomposition into parent binary and/or ternary phases [57].

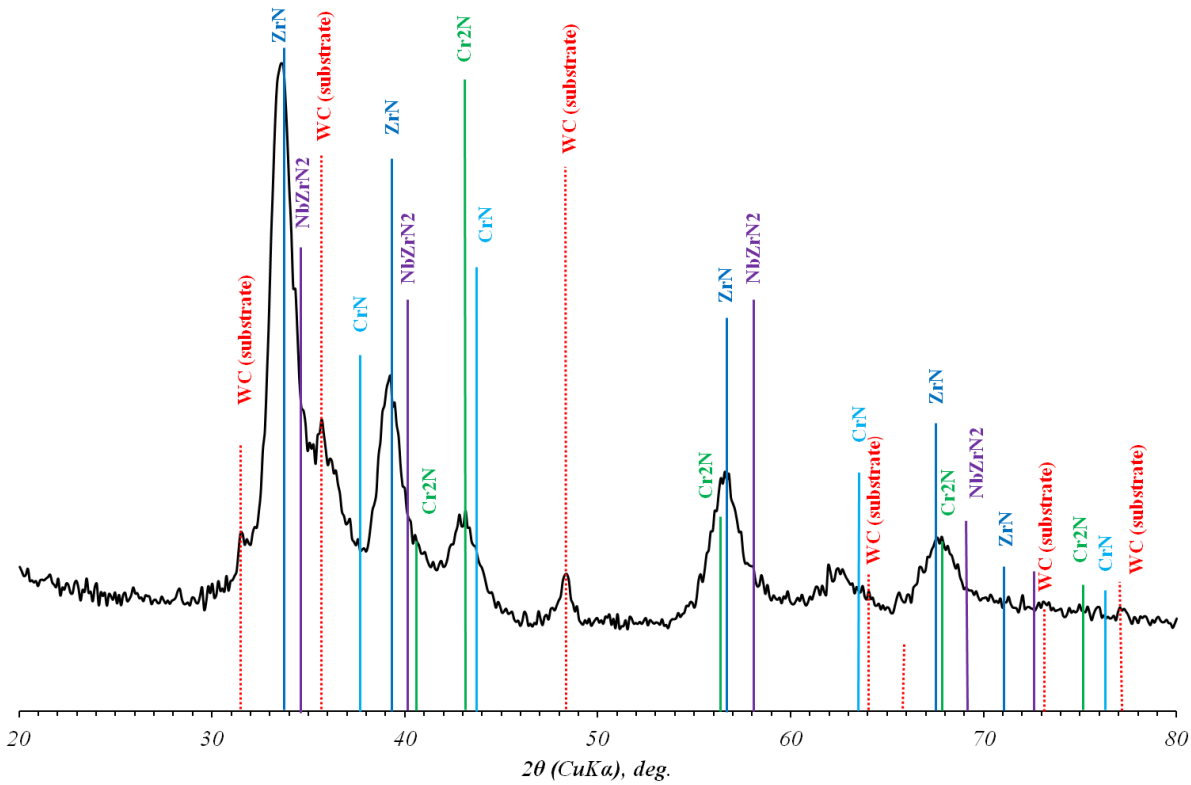

Fig. 6. XRD pattern of Zr-ZrN-(Nb,Zr,Cr,Al)N coating on WC-Co substrate

Sample with Zr-ZrN-(Zr,Al,Si)N coating

A diffraction pattern of Zr-ZrN-(Zr,Al,Si)N is shown in Fig. 7. The coating includes a ZrN phase (space group Fm-3m, a=4,5978 Å), which is most likely a solid solution of Al in ZrN, as evidenced by the shift of the lines with respect to the reference data. Lines of Zr sublayer are not detected on the XRD pattern due to their low intensity.

All diffraction patterns shown in Fig. 5-7 also contain reflections from the WC substrate main phase.

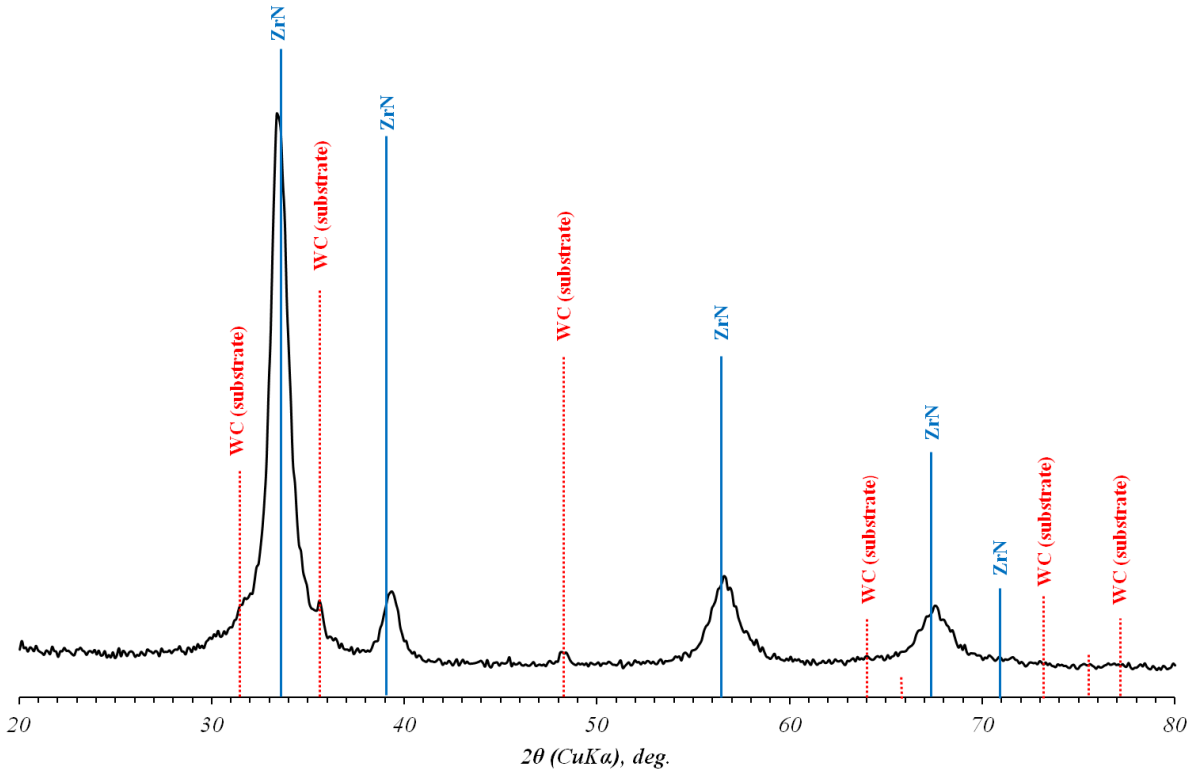

Fig. 7. XRD pattern of Zr-ZrN-(Zr,Al)N coating on WC-Co substrate

Study of strength of adhesion and cohesion bonds by scratch testing

Figures 8-12 present the graphs of changes in load and acoustic emission signal, as well as panoramas of scratches on samples and fragments of scratches at the start of coating failure (at load L_{C1}) and complete coating failure (at load L_{C2}).

On the sample with Ti-TiN-(Ti,Cr,Al,Si)N coating (Fig. 8.), the failure mode of wedging spallation can be observed [58]. The coating started to fail at L_{C1} = 32 N, while complete failure occurred at L_{C2} = 36 N. The complete coating failure means overall failure of wear-resistant layer (Ti,Cr,Al,Si)N, while transitional layer TiN bears no visible signs of failure. When layer (Ti,Cr,Al,Si)N fails, the process of failure can be observed as formation of a grid of cracks (Fig. 8 Area I, 1) or as elements of plastic deformation upon movement of an indenter (Fig. 8. Area I, 2). When critical load value of L_{C2} is reached, the mechanism of brittle failure prevails with formation of through cross-section cracks running through layer (Ti,Cr,Al,Si)N (Fig. 8. Area II,3,4,5).

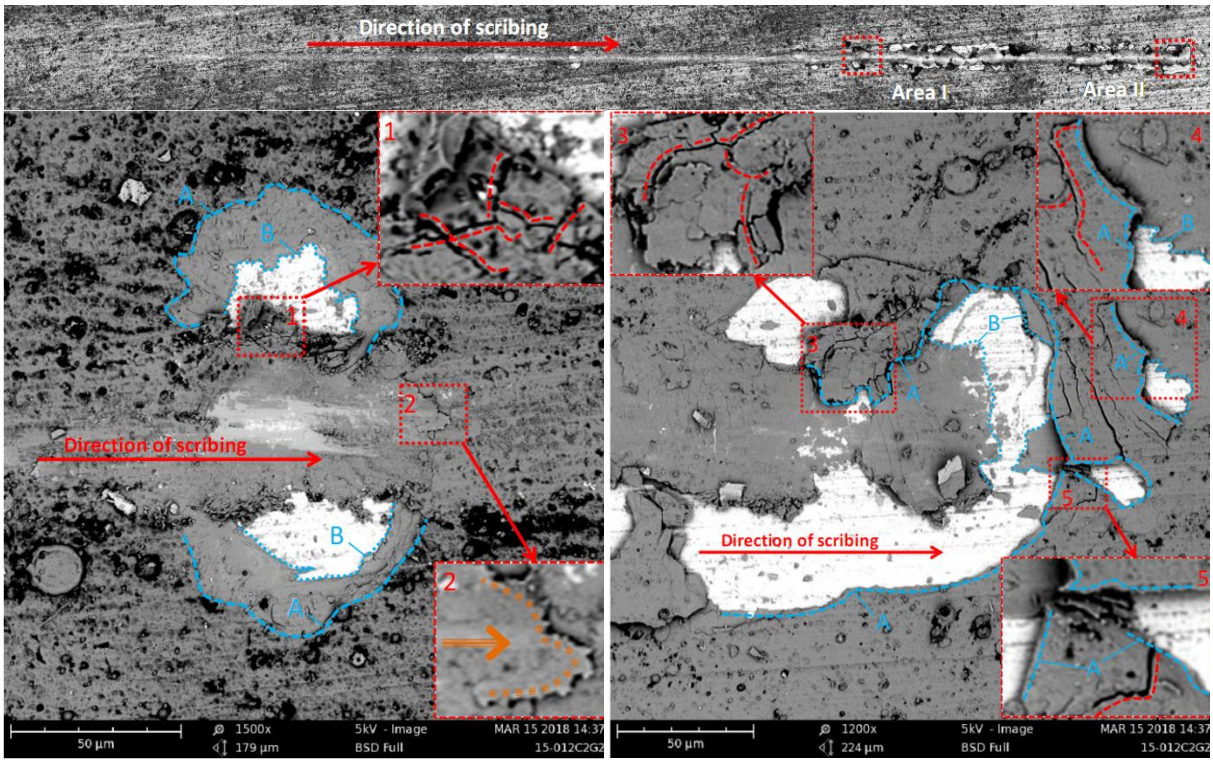

Area I Area II

Fig. 8. Panorama of a scratch (on top) and a fragment of a scratch in the place where Ti-TiN-(Ti,Cr,Al,Si)N coating starts to fail (Area I) and complete destruction (Area II). A – border of coating failure area; B – border of outer wear resistant layer (Ti,Cr,Al,Si)N and transitional layer TiN of the coating.

Let us consider the failure mode for Ti-TiN-(Ti,Cr,Al,Si)N coating on cross cut made in a plane perpendicular to the direction of scribing in the area of starting failure at load of L_{C1} = 32 N (Fig. 9). In the central part of the scribing groove, an area of elastic plastic deformation is clearly seen. Fig. 9. Area C shows preserved coating in the central part of the scribing groove (the loss of the coating in the foreground occurred during the cut and is not related to the scribing process). Delamination of the coating in combination with cracking and brittle failure occurs at the borders of the central area of the elastic plastic deformation (Fig. 9.Area B), and that also correlates with Fig. 8. Area I – 1. There is also an area of tear-out of the embedded microdroplet D. At the same time, no delamination is observed from the other side of the scribing groove, and plastic deformation may be noted as the dominating mechanism of the coating failure (Fig. 9. Area A). In this case, the dashed line indicates the border of outer wear resistant layer (Ti,Cr,Al,Si)N and transitional layer TiN of the coating.

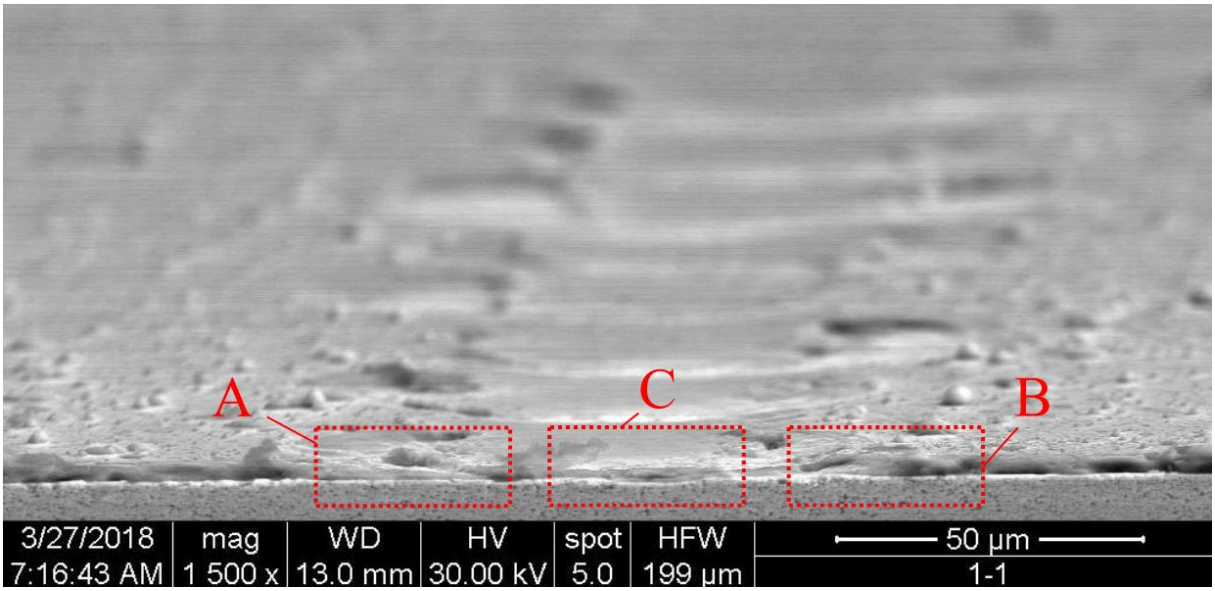
A
C
B
3/27/2018
7:16:43 AM
mag
1 500 x
WD
13.0 mm
HV
30.00 kV
spot
5.0
HFW
199 µm
50 µm
1-1

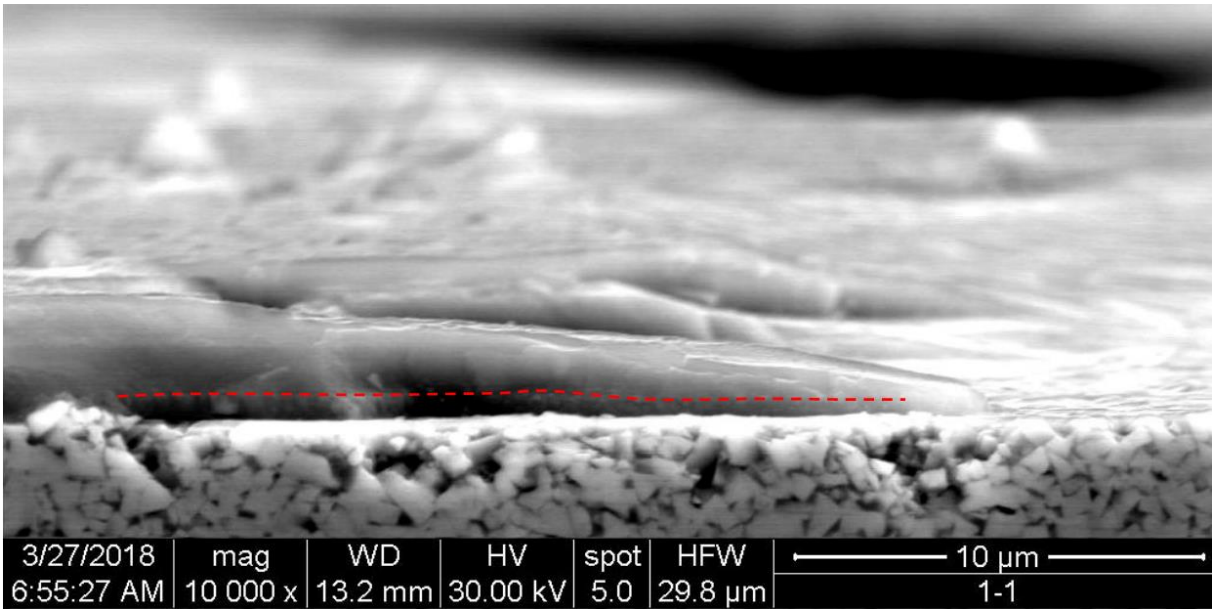
3/27/2018
6:55:27 AM
mag
10 000 x
WD
13.2 mm
HV
30.00 kV
spot
5.0
HFW
29.8 µm
10 µm
1-1

Area A

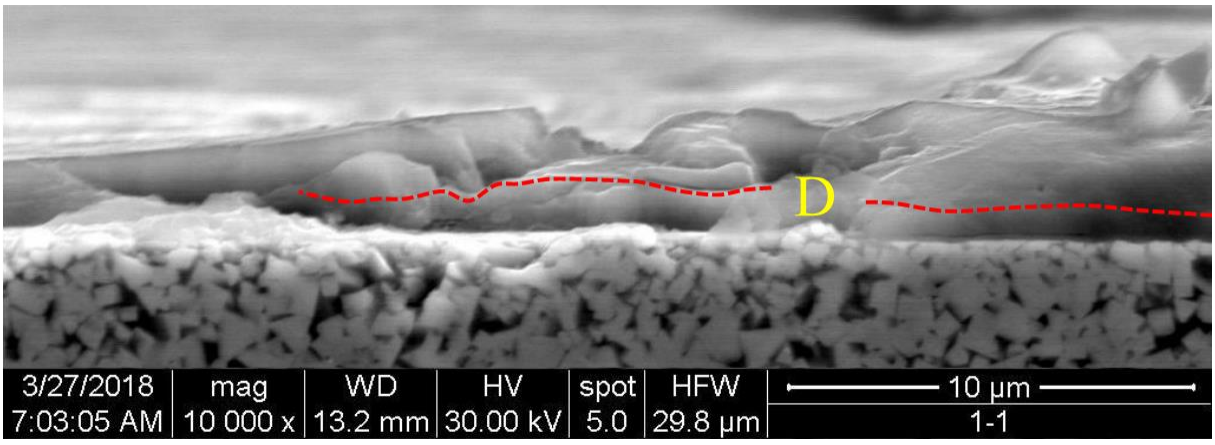
D
3/27/2018
7:03:05 AM
mag
10 000 x
WD
13.2 mm
HV
30.00 kV
spot
5.0
HFW
29.8 µm
10 µm
1-1

Area B

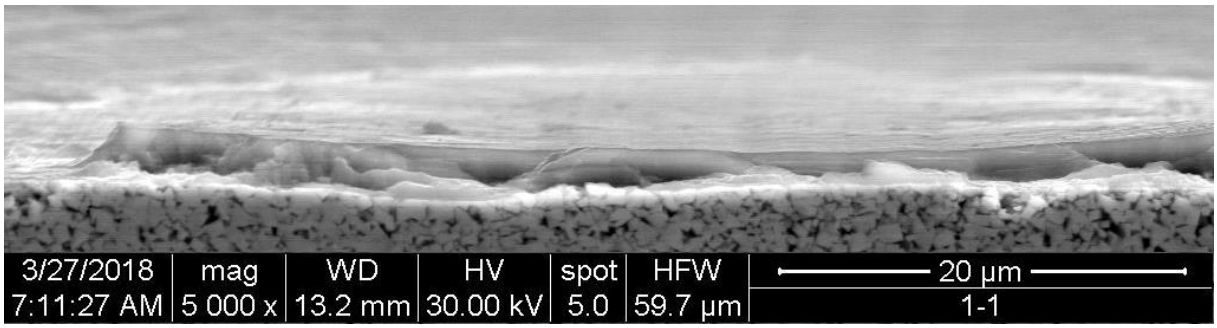

Area C

Fig. 9. Cross cut of carbide substrate with Ti-TiN-(Ti,Cr,Al,Si)N coating in the area of starting failure at load of L_{C1} = 32 N. General view (a) and area with elements of delaminations and brittle failure (b). A – border of coating failure area; 2 – border of area where plastic deformation of the coating occurs.

Zr-ZrN-(Nb,Zr,Cr,Al)N coating demonstrated the lowest adhesion resistance. Coating failure occurred as recovery spallation, and it was accompanied by tearing of large sections of the coating (Fig. 10.). Spalled edges of the coating demonstrate moire pattern, formed in failure of individual layers of the coating. The first centres of failure appeared at load L_{C1} = 16 N, and the complete coating failure occurred at L_{C2} = 29 N. For this coating, a clear mechanism of brittle failure is typical. Meanwhile, there is formation of through cross-section cracks in layer (Nb,Zr,Cr,Al)N (Fig. 10. Area I, 2), as well as grinding of surface layer with formation of small fragmentation area (Fig. 10. Area I, 3; Fig. 10. Area II, 5). An important failure feature typical for this coating is in formation of cracks in planes located at an angle to surface of the coating (Fig. 10. Area I, 1,4). Such cracks are characterized by a combination of discontinuities in nanolayers with delaminations between nanolayers. The result of such failure is in typical "moire" structure clearly visible on zoomed inserts (Fig. 10. Area I, 1,4). Meanwhile, at critical load L_{C1}, wear-resistant layer (Nb,Zr,Cr,Al)N fails till the border of intermediate sublayer (Nb,Zr,Cr)N (dashed line B1). When critical load L_{C2} is reached, nanolayers of wear-resistant layer (Nb,Zr,Cr,Al)N below intermediate sublayer (Nb,Zr,Cr)N (dashed line B2) fail up to the border with transitional layer ZrN (dashed line B).

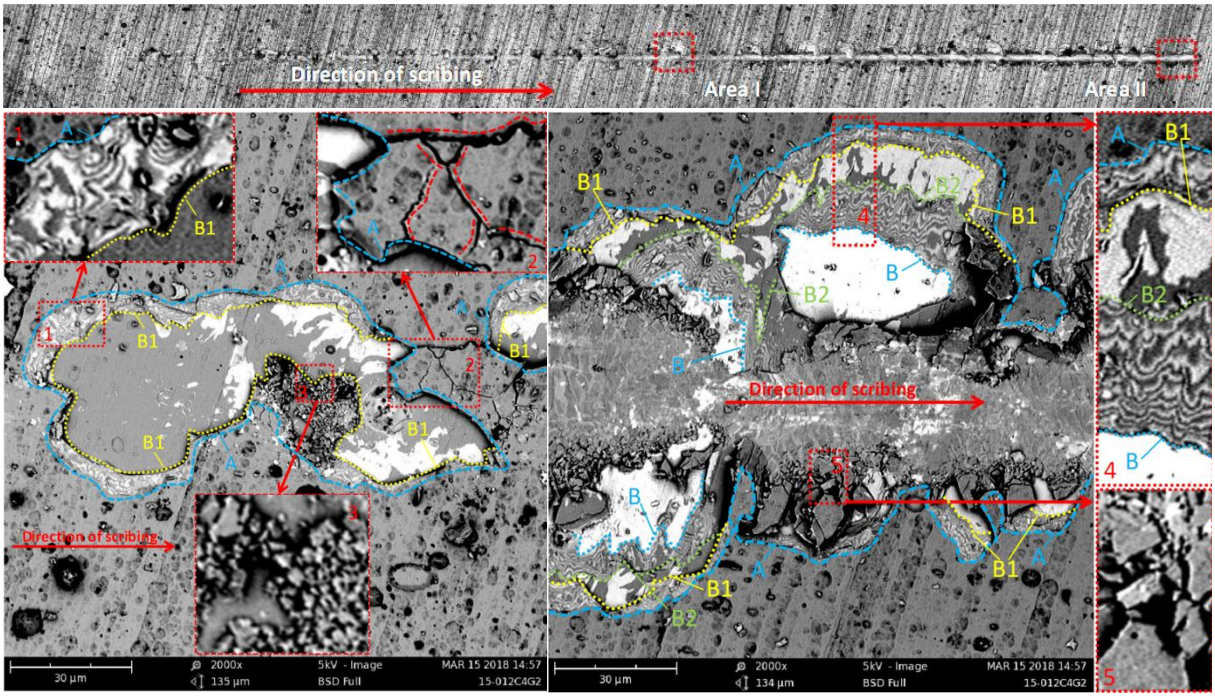

Area I Area II

Fig. 10. Panorama of a scratch (on top) and a fragment of a scratch in the place where Zr-ZrN-(Nb,Zr,Cr,Al)N coating starts to fail (Area I) and complete destruction (Area II). A – border of coating failure area; B1 – border of "external area of wear-resistant layer" (Nb,Zr,Cr,Al)N – intermediate sublayer (Nb,Zr,Cr)N»; B2 – border of "intermediate sublayer (Nb,Zr,Cr)N – internal area of wear-resistant layer (Nb,Zr,Cr,Al)N"; B – border of outer wear resistant layer (Nb,Zr,Cr,Al)N and transitional layer ZrN of the coating.

Let us consider the failure mode for ZrN-(Nb,Zr,Cr,Al)N coating on cross cut made in a plane perpendicular to the scribing direction in the area of starting failure at load of L_{C1} = 16 N (Fig. 11). In the central part of the scribing groove, an area of elastic plastic deformation is clearly seen (the border of the area is indicated by the dashed line 2). At the same time, elements of delamination and brittle failure are clearly visible (Fig. 11. b).присутствуют явно выраженные элементы деламинации и хрупкого разрушения (Fig. 11. b).

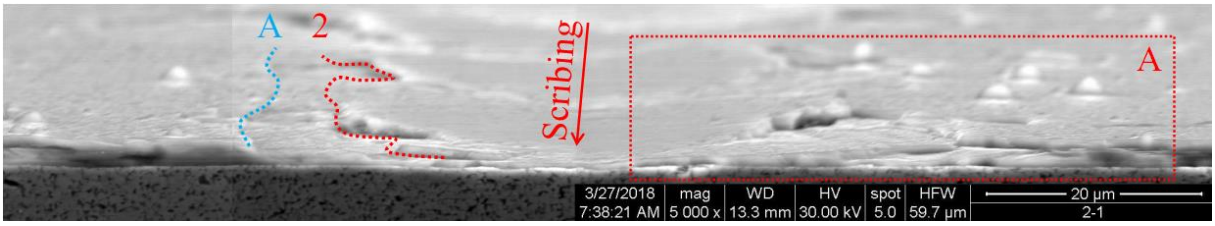

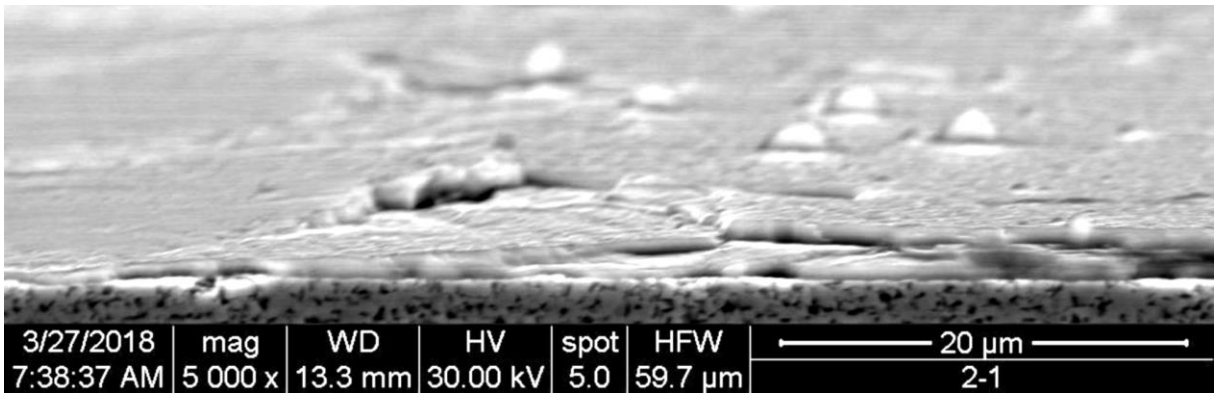

Area A

Fig. 11. Cross cut of carbide substrate with ZrN-(Nb,Zr,Cr,Al)N coating in the area of starting failure at load of L_{C1} = 16 N. General view (from above) and area with elements of delaminations and brittle failure (Area A). A – border of coating failure area; 2 – border of area where plastic deformation of the coating occurs.

Zr-ZrN-(Zr,Al,Si)N coating is characterized by the highest adhesion resistance. Its start of failure can be observed as chipping at L_{C1} = 17 N, and no complete coating failure occurs at maximum load of 40 N, used in these experiments (Fig. 12.). The failure process for this coating shows clear plastic deformation along the move of an indenter (in particular, Fig. 12. Area I, 1). Meanwhile, there are also areas of spallation of external part of wear-resistant layer (Zr,Al,Si)N from intermediate sublayer ZrN. At the same time, there are also local delaminations between nanolayers of external part of wear-resistant layer (Fig. 12. Area II, 2,3). No failure of nanolayers of wear-resistant layer below transitional layer and intermediate layer ZrN occurs at this maximum load (40 N).

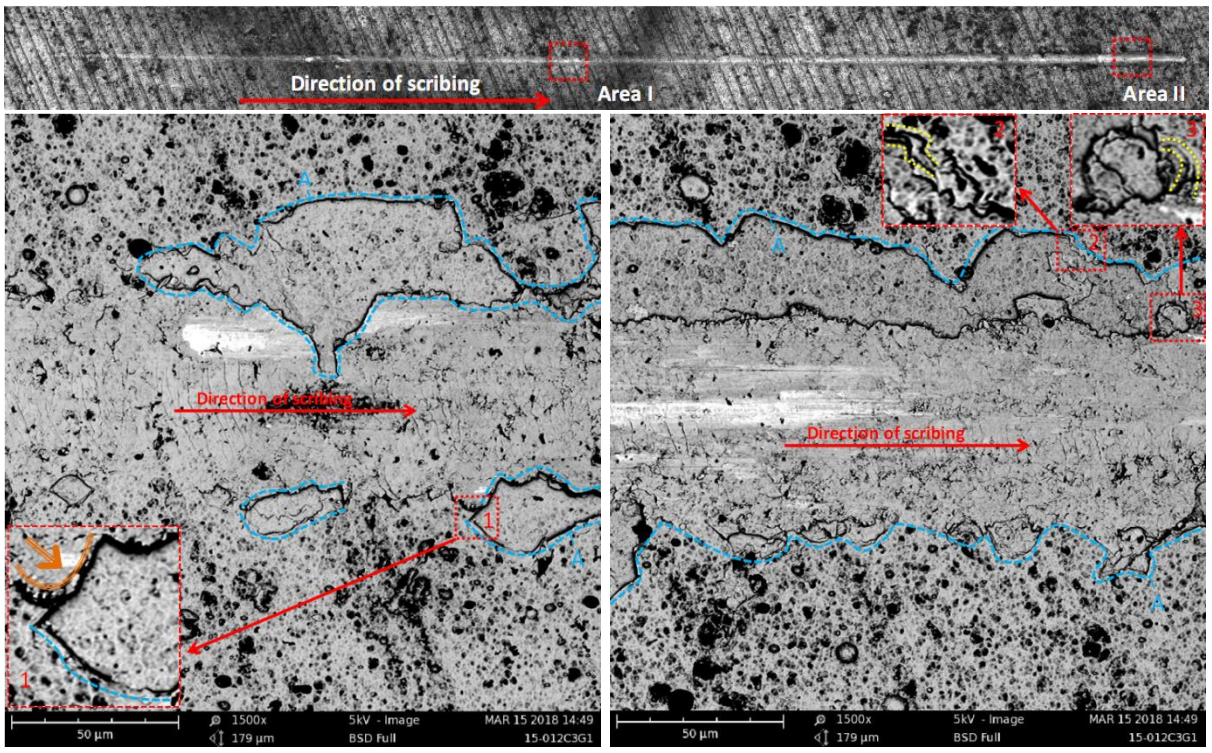

Area I Area II

Fig. 12. Panorama of a scratch (on top) and a fragment of a scratch in the place where Zr-ZrN-(Zr,Al,Si)N coating starts to fail (Area I) and complete destruction (Area II). A – border of coating failure area;

Thus, the thicker sublayer with low content of aluminum introduced in the structure of nanolayered coating produces no significant effect of the failure mode of the coating in case when the thickness of such sublayer is about 2 times higher than average thickness of nanolayers (Ti-TiN-(Ti,Cr,Al,Si)N). For Zr-ZrN-(Zr,Al,Si)N coating, in which the thickness of sublayer with low content of aluminum is about 4 higher than average thickness of nanolayers, local spallations are observed along external border of the above sublayer. Finally, for Zr-ZrN-(Nb,Zr,Cr,Al)N coating, in which the sublayer under the study has thickness about 9 times higher than average thickness of nanolayers, there are significant delaminations along the external border of the above sublayer. Proceeding from the above, it can be concluded that when nanolayers differ in their thickness in more than 2 times that can negatively affect wear resistance of the coating.

Study of tribological parameters of coated samples at elevated temperatures

The temperature range of 450-950°C has been arranged to study the influence of temperature on tribotechnical properties of tribopairs of "the material being machined–cutting tool with coating" (shear strength τ_n of adhesion bonds, normal stress on contact P_n, and relation $\frac{\tau_n}{P_n}$, which in fact represents the adhesion component of the COF, on which the deeper deformation of contact layers depends [F_1, F_2]). The graphs of relation between τ_n, P_n and $\frac{\tau_n}{P_n}$ and temperature are presented in Fig. 13. It can be seen from the above relations that the shear stresses τ_n initially grow for all the samples and then decrease with an increase in temperature.

Let us consider the features of the change in the adhesion (molecular) component f_M of the friction coefficient with increasing temperature. It should be noted that the parameter value for samples with coatings is noticeably lower than for an uncoated sample at all temperatures and for all types of carbides.

During the study of the change in f_M upon a contact with counterbody of steel AISI 321 (Fig. 13), it can be seen that the dynamics in the change of f_M is similar for all samples: at first, the value of f_M increases, but after reaching a certain temperature, it begins to decrease. However, the value of temperature, after which f_M begins to decrease is different for different samples. In particular, for a sample with ZrN-(Nb,Zr,Cr,Al)N coating, such a decrease starts after temperature reaches 750 °C, while for a sample with Ti-TiN-(Ti,Cr,Al,Si)N coating after temperature reaches 850 °C. If in contact with a counterbody of steel AISI 321, a sample with Ti-TiN-(Ti,Cr,Al,Si)N coating shows the highest value of f_M among all the samples. Meanwhile, for the rest samples, the dynamics of the change in f_M depending on temperature is largely monotonous for both the counterbody materials under the study. A sample of Zr-ZrN-(Zr,Al,Si)N coating showed the lowest change in f_M with an increase in temperature above 800 °C.

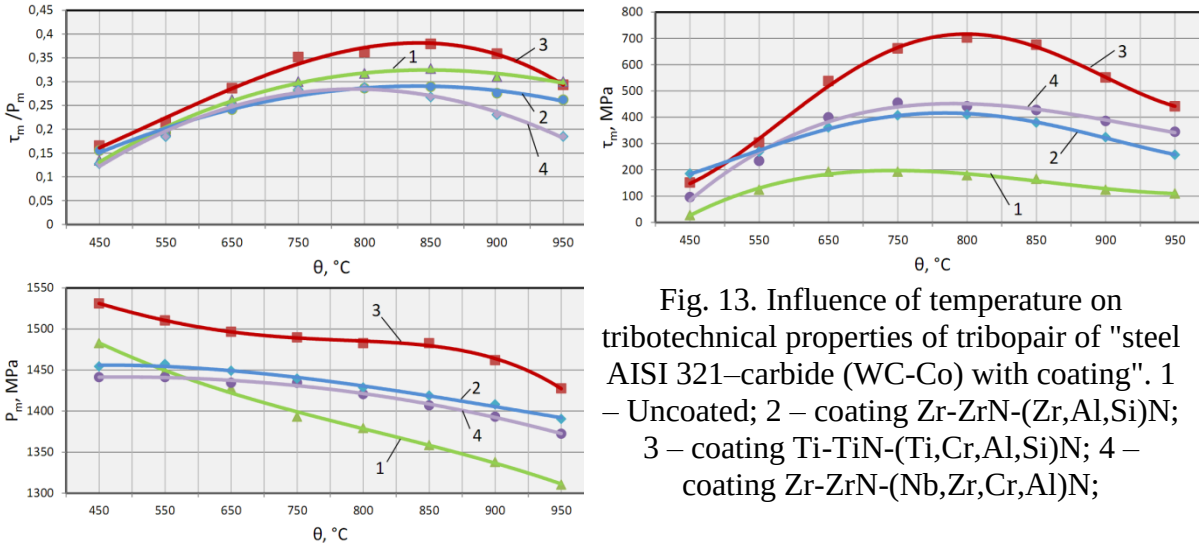

Fig. 13. Influence of temperature on tribotechnical properties of tribopair of "steel AISI 321–carbide (WC-Co) with coating". 1 – Uncoated; 2 – coating Zr-ZrN-(Zr,Al,Si)N; 3 – coating Ti-TiN-(Ti,Cr,Al,Si)N; 4 – coating Zr-ZrN-(Nb,Zr,Cr,Al)N;

Cutting tests

The results of cutting tests in steel AISI 321 longitudinal turning by carbide (WC-Co) tools (uncoated and with the coatings under the study) are presented in Fig. 14. Tool with Ti-TiN-(Ti,Cr,Al,Si)N coating shows longer tool life; however, approximately during the last quarter of the wear resistance period, the dynamics of tool wear for a tool with the above coating intensifies significantly. Meanwhile, a tool with Zr-ZrN-(Zr,Al,Si)N coating shows more stable wear behavior and less intensive wear at the end of the wear resistance period. This results correlates well with the data on the change in the adhesion component of COF f_M with an increasing temperature (see Fig. 14, as well as the highest strength of adhesion bond to substrate of the coating (L_{C2}>40 N). As tool wear increases, a temperature in cutting zone increases, and values of f_M change respectively. It is important to note that a tool with Zr-ZrN-(Zr,Al,Si)N coating with sufficiently low value of f_M at high temperatures and the highest value of L_{C2} showed the longest tool life in turning. Meanwhile, a tool with Ti-TiN-(Ti,Cr,Al,Si)N coating with the highest value of f_M and average value of L_{C2} (36 N) showed even slightly longer tool life till cutting path reached 12,000 m, and only after that the tool with the above coating showed more active wear. As a result, a tool with Ti-TiN-(Ti,Cr,Al,Si)N coating showed the second result in tool life. And finally, a tool with Zr-ZrN-(Nb,Zr,Cr,Al)N coating showed the lowest value of f_M at high temperatures and the worst strength of adhesion bond to substrate (29 N). A tool with the above coating showed the shortest tool life among all the tools with the coatings under the study. Accordingly, it can be argued that the strength of adhesion bond to substrate L_{C2}, measured at room temperature, produces a greater effect on tool life of a coated tool than adhesion component of COF f_M, measured at high temperatures, at least for the cutting conditions under consideration.

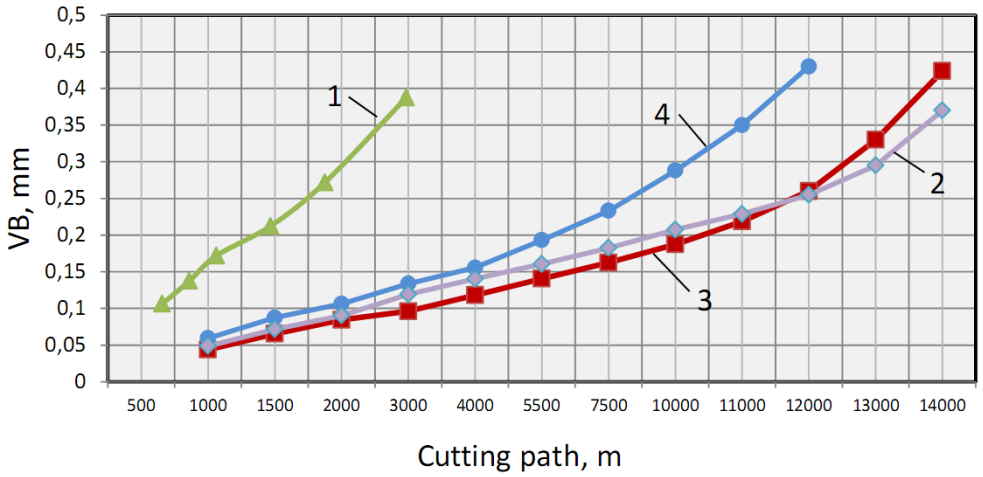

Fig. 14. Effect produced by the length of cutting path on flank wear land when turning steel AISI 321 at f = 0.20 mm/rev; a_p = 0.5 mm; v_c = 300 mmin-1.
1 – Uncoated carbide (WC-Co); 2 – coating Zr-ZrN-(Zr,Al,Si)N; 3 – coating Ti-TiN-(Ti,Cr,Al,Si)N; 4 – coating Zr-ZrN-(Nb,Zr,Cr,Al)N

Study of wear mechanisms for coated samples after cutting tests

Let us consider a pattern of wear of a carbide tool with the coatings under the study in machining of steel AISI 321 (Fig. 15, 16). For an uncoated tool, formation of a large wear crater on rake face is typical, and that can indicate a high temperature in the cutting zone and intensive adhesion between rake face of cutting tool and chips. For a cutting tool with Zr-ZrN-(Zr,Al,Si)N coating, a wear crater also forms on rake face, but it is significantly less clear, and it can be stated that flank wear land is the limiting form of wear. For a tool with Ti-TiN-(Ti,Cr,Al,Si)N coating, a wear crater is even more clear, but flank wear land is also the limiting form of wear. In general, Zr-ZrN-(Zr,Al,Si)N and Zr-ZrN-(Nb,Zr,Cr,Al)N coatings show very similar wear mechanism with formation of almond-shaped wear craters extended along cutting edge and limiting wear on flank face. For a tool with Ti-TiN-(Ti,Cr,Al,Si)N coating, a wear crater on rake face is more extended in direction of chip removal, and that can be clearly seen in Fig. 16. This fact can be explained by the higher value of f_M and, respectively, by longer contact zone of the chips with rake face. Meanwhile, flank wear land is a limiting factor rather than formation of clear wear crater. It can be stated that Zr-ZrN-(Nb,Zr,Cr,Al)N coating provides minimal adhesion to the material being machined, and that is confirmed by low values of COF f_M at temperatures corresponding to temperatures in the cutting zone (see Fig. 15). Meanwhile, in contact with a counterbody of steel AISI 321, the Ti-TiN-(Ti,Cr,Al,Si)N coating show sufficiently high vales of f_M, with the maximum among all the samples under the study in a temperature range of 450-950 °C, and it begins to decrease noticeable only at temperatures above 950 °C. This fact indicates that f_M of the friction coefficient produces a significant effect on the dynamics of tool wear in cutting. However, this parameter is undoubtedly not the only factor affecting the cutting process and the dynamics of cutting tool wear.

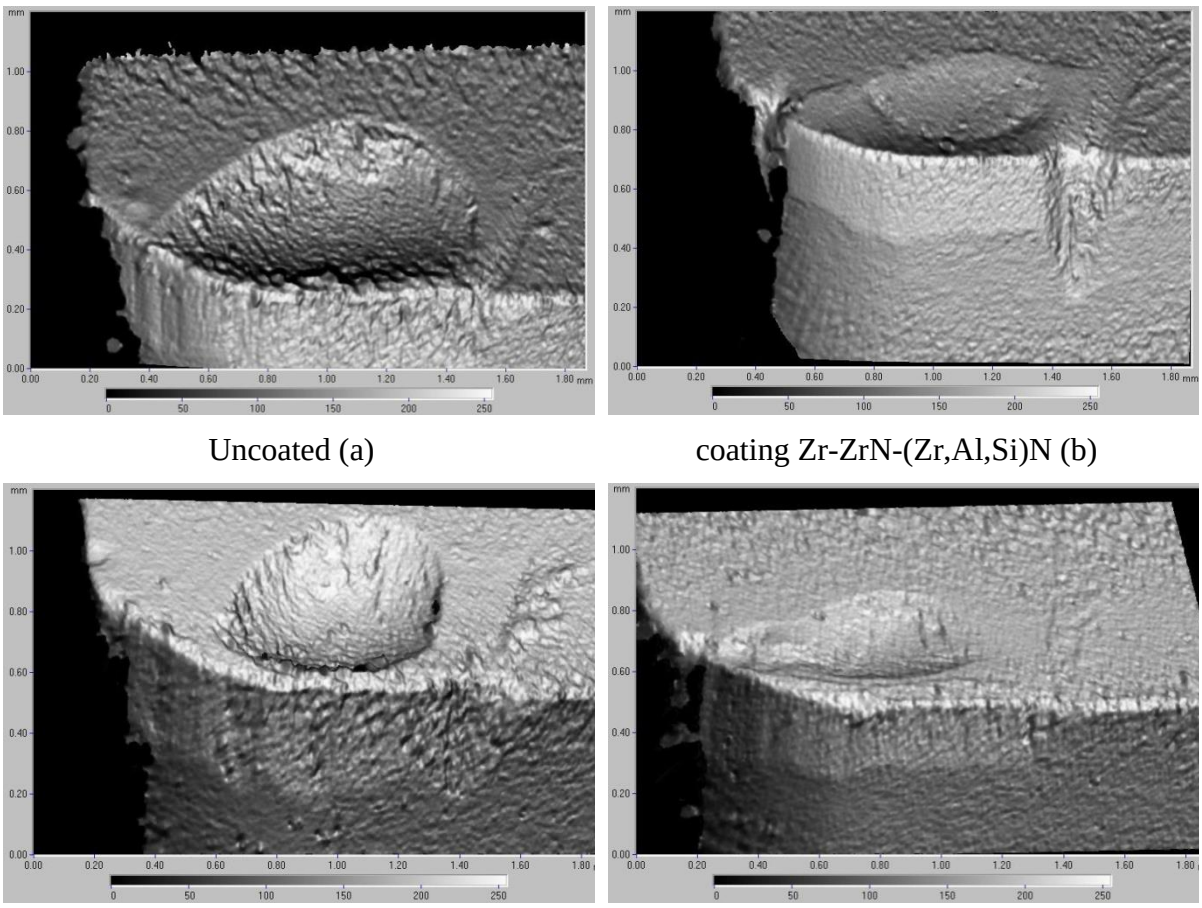

Uncoated (a) coating Zr-ZrN-(Zr,Al,Si)N (b)

coating Ti-TiN-(Ti,Cr,Al,Si)N (c) coating Zr-ZrN-(Nb,Zr,Cr,Al)N (d)

Fig. 15. Pattern of wear of a carbide tool with coatings under the study in turning of steel AISI 321 at f = 0.20 mm/rev; a_p = 0.5 mm; v_c = 300 mmin-1 (obtained through MicroCAD optical 3D measuring system).

Fig. 16 shows a picture of rake face of carbide inserts with the coatings under the study with indication of a cross section plane. The ideal place for a section is in the widest part of wear crater; however, the available techniques do not allow making a section with such high location accuracy. Accordingly, a wear crater section in Fig. 17, 18 and 19 do not reflect its actual maximum width.

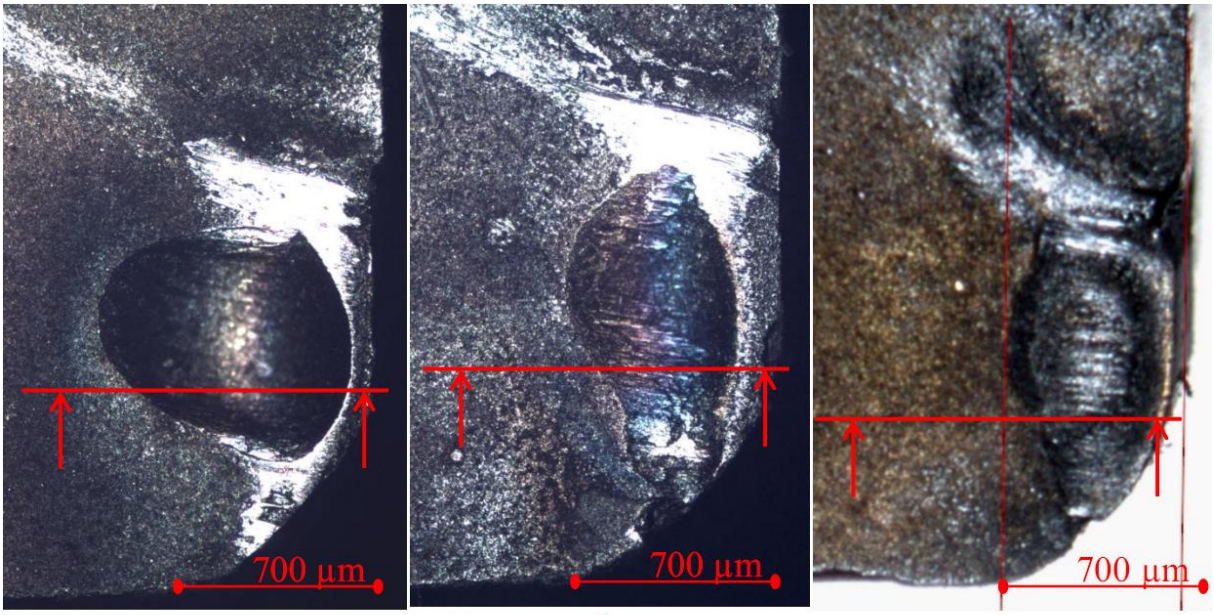

Fig. 16. A picture of rake face of a carbide insert with the coatings under the study, with indication of cut section plane for a tool with Ti-TiN-(Ti,Cr,Al,Si)N coating after 12,000 m of cutting path (a); with Zr-ZrN-(Nb,Zr,Cr,Al)N coating after 14,000 m of cutting path (b); with Zr-ZrN-(Zr,Al,Si)N coating after 14,000 m of cutting path; (c) when turning steel AISI 321 at f = 0.20 mm/rev; a_p = 0.5 mm; v_c = 300 mmin-1.

Let us consider the failure mode of the coatings under the study on cross cut (Fig. 17-20). A tool with Ti-TiN-(Ti,Cr,Al,Si)N coating is characterized by a combination of abrasive and adhesive wear in areas, directly adjacent to cutting edge (Fig. 17. III) or to a wear crater (Fig. 17. I). Meanwhile, there is active cracking with formation of through cross-cut cracks, which in some cases stop at the border of "wear-resistant layer-transitional layer" (Fig. 18. II). The failure mode with formation of cross-cut cracks is well correlated with the data obtained in scratch testing (Fig. 8). No delaminations are observed between layers and nanolayers of the coating. In the area, directly adjacent to the cutting edge (Fig. 17. I,III), there is abrasion of surface nanolayers of the coating, while the border of wear passes along the external border of intermediate sublayer (Ti,Cr)N or slightly above this sublayer.

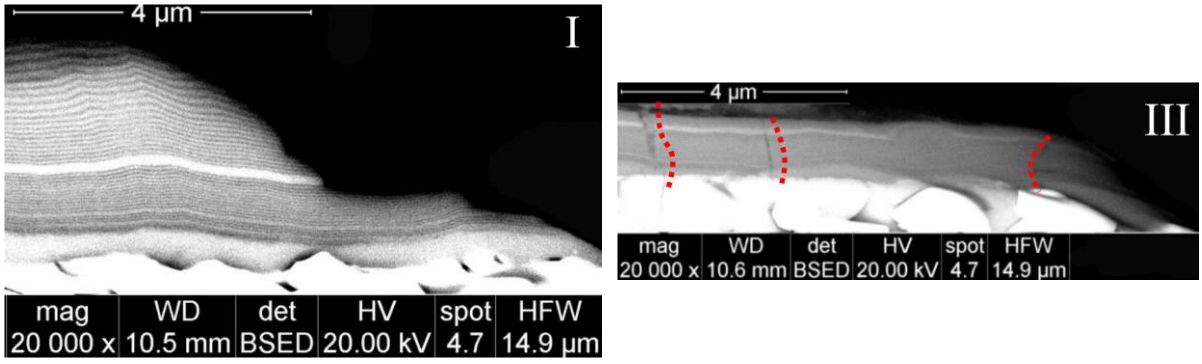

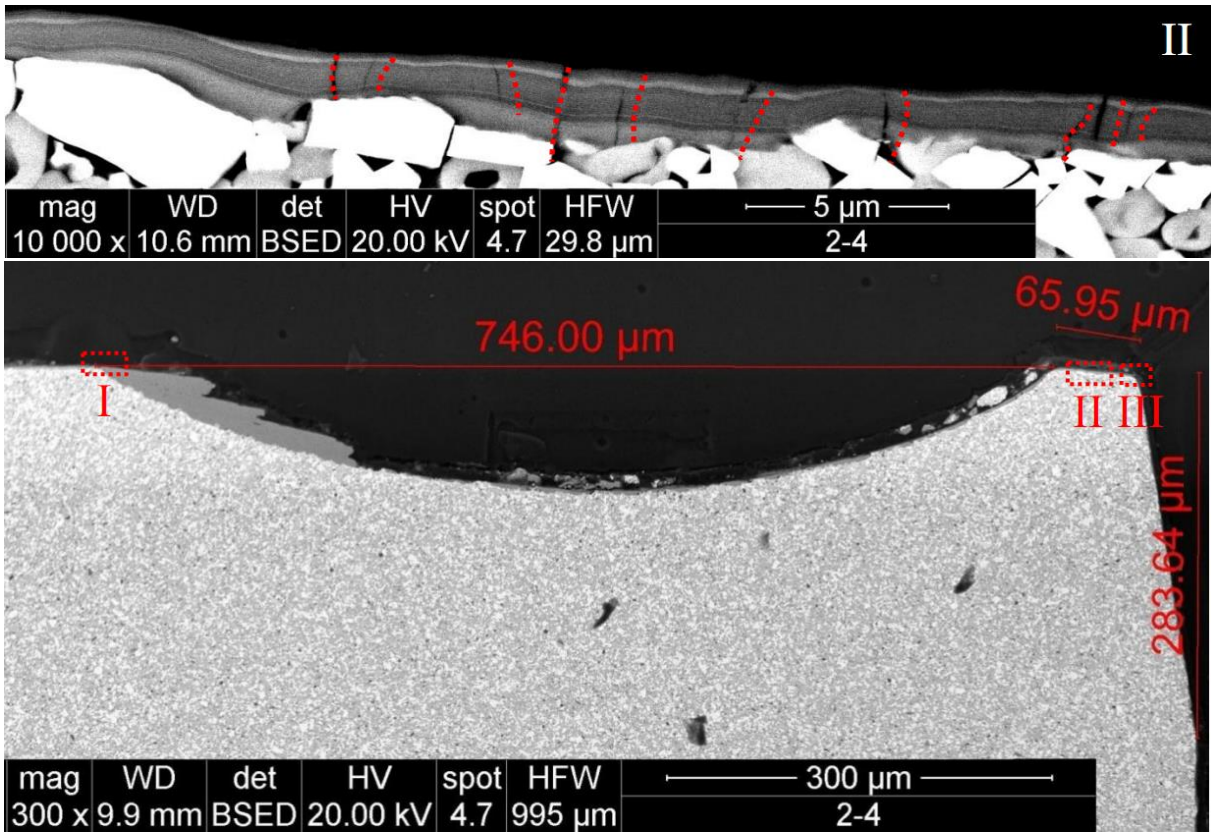

Fig. 17. Microstructure of a tool with Ti-TiN-(Ti,Cr,Al,Si)N coating on cross cut.

A tool with Zr-ZrN-(Nb,Zr,Cr,Al)N coating is also characterized by the abrasive and adhesive wear mechanism and formation of through cross-cut cracks in areas, directly adjacent to cutting edge (Fig. 18. I). At the same time, in the area, adjacent to a wear crater, there are delaminations on the border of "transitional layer-wear-resistant layer", as well as delaminations between nanolayers (Fig. 18. II).

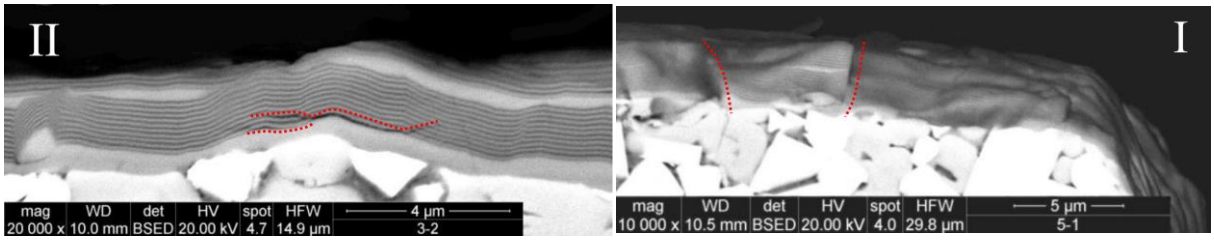

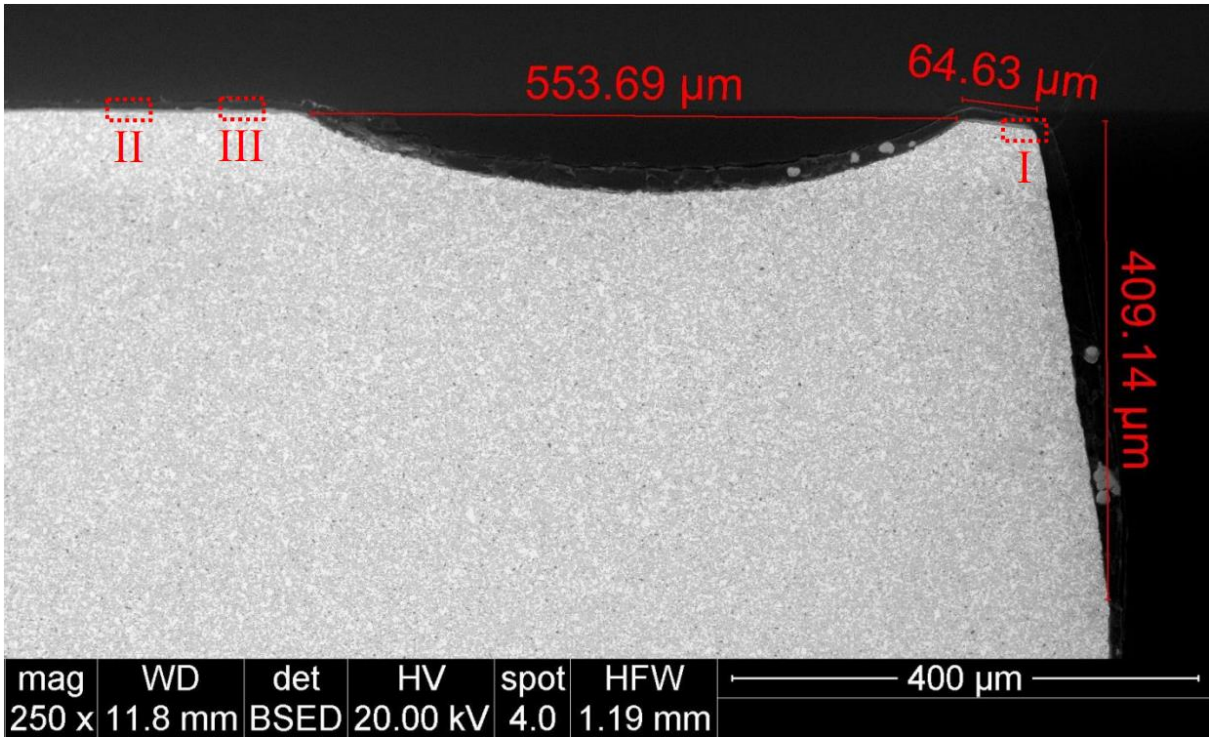

Fig. 18. Microstructure of a tool with Zr-ZrN-(Nb,Zr,Cr,Al)N coating on cross cut.

Let us consider separately Area III (Fig. 18), which is characterized by adherent pieces of the material being machined (Fig. 19). When coating surface interacts with chips, significant shear stresses occur on rake face of a tool, and in this case they led to formation of extensive delamination, mainly formed along the border "intermediate sublayer (Nb,Zr,Cr)N–external area of wear-resistant layer (Nb,Zr,Cr,Al)N". This failure mode demonstrated by Zr-ZrN-(Nb,Zr,Cr,Al)N coating correlates well with the results obtained in scratch testing (Fig. 10). Another typical feature of the failure shown by this coating is in formation of cracks in planes located at an angle to surface of the coating, and that also correlates with the results obtained in scratch testing (Fig. 10). A noticeable effect on the coating failure is also produced by microdroplets D (Fig. 19).

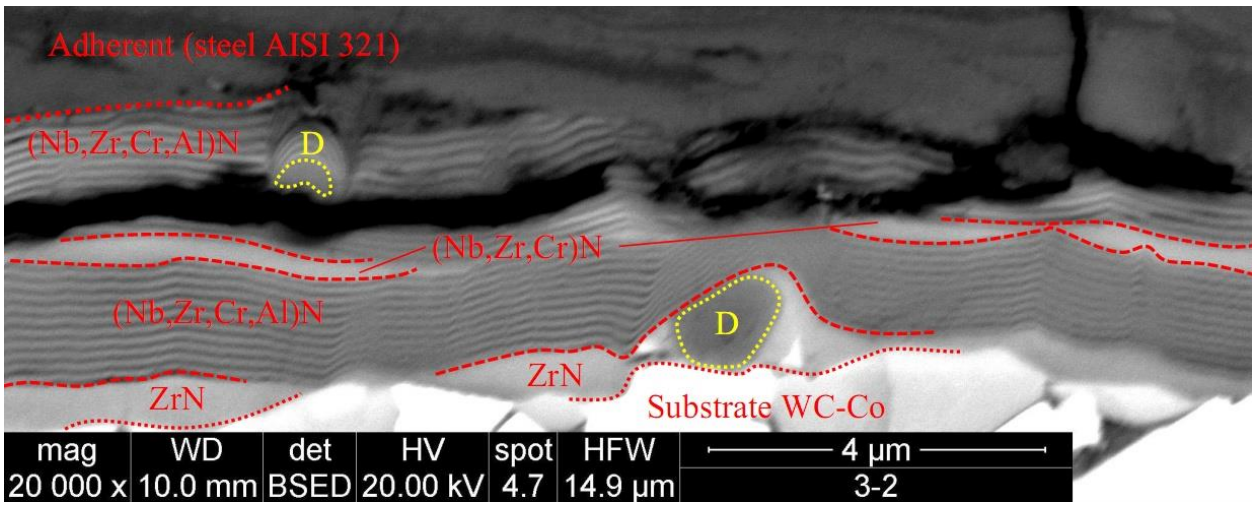

Fig. 19. Microstructure of a tool with Zr-ZrN-(Nb,Zr,Cr,Al)N coating on cross cut. D – microdroplets Zr embedded to the coating structure.

A tool with Zr-ZrN-(Zr,Al,Si)N coating is characterized by abrasive and adhesive wear behavior. In area of rake face, directly adjacent to cutting edge, there is abrasive and adhesive wear of coating up to external border between intermediate and next sublayers, with approach of cutting edge, abrasion of the coating, up to its complete failure (Fig. 20. I). Meanwhile, no formation of cracks and delaminations are observed (Fig. 20. I,II).

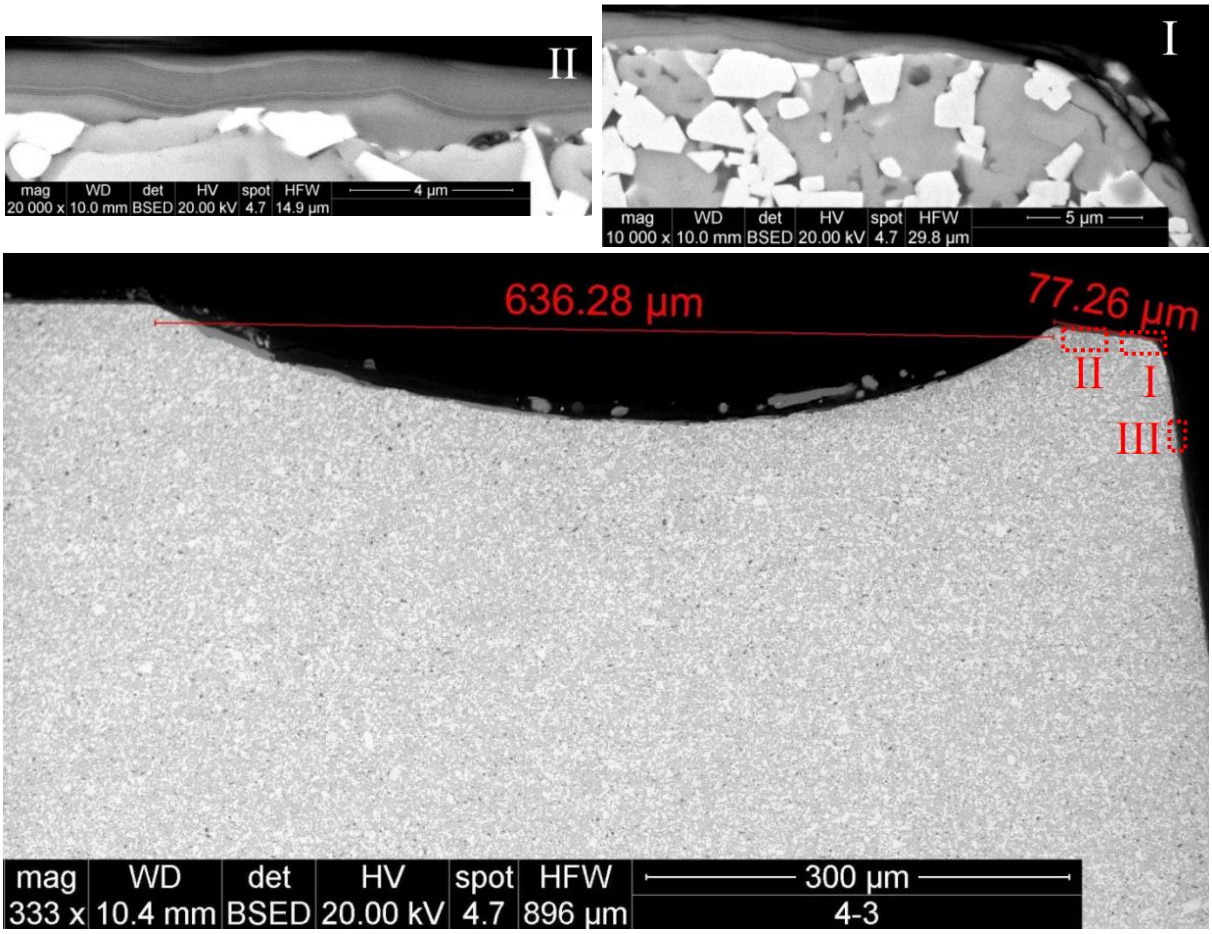

Fig. 20. Microstructure of a tool with Zr-ZrN-(Zr,Al,Si)N coating on cross cut.

Let us consider separately the failure mode of Zr-ZrN-(Zr,Al,Si)N coating on flank face of a tool, in particular, in the area (Fig. 20. III). Fig.21 presents a micrograph of cross cut of a section on flank face of a tool with Zr-ZrN-(Zr,Al,Si)N coating. In this case, under the action of compressive stresses, acting along flank face of the tool, a series of delaminations are formed between nanolayers of the coating. Meanwhile, no delamination along the borders of the intermediate sublayer, as well as interlayer delaminations and spallation of the coating from the substrate are observed. The failure mode demonstrated by this coating indicates its sufficiently high plasticity in combination with a high level of adhesive and cohesive bonds. This result correlates with the above results obtained in scribing.

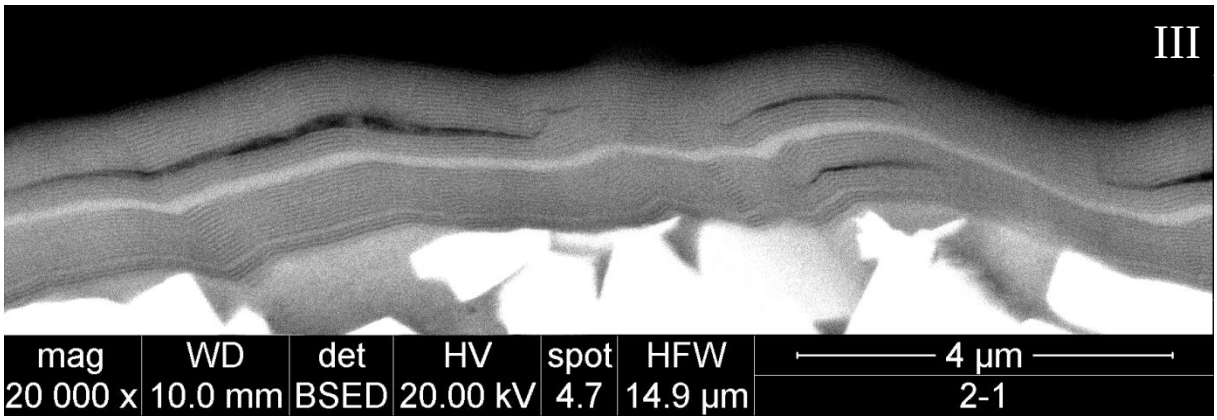

Fig. 21. Cross-cut of a section of flank face in a tool with Zr-ZrN-(Zr,Al,Si)N coating (with rotation of 90°) (Area III at Fig. 20).

CONCLUSIONS

The processes occurring in the cutting zone are very sophisticated, and it is very difficult to simulate them. So far, no ideal model (mathematical or mechanical) to take into account all the factors of the process (including stresses, temperature, diffusion and chemical processes, etc.) has been ever created and it is unlikely to be created in the near future. Accordingly, a completely adequate assessment of the coating performance can only be made through cutting tests. Meanwhile, there are a number of methods, including those considered in this article, to predict the performance properties of coatings with a fairly high probability.

The conducted studies found out the following:
- the coatings under the study demonstrate formation of complex phases, in particular, $NbZrN_2$ and $CrTiN_2$, which can produce a significant effect on the performance properties of the coatings;
- a sample with Zr-ZrN-(Zr,Al,Si)N coating is characterized by the maximum strength of adhesion bond to substrate (L_{C2}>40 N), while a sample with Ti-TiN-(Ti,Cr,Al,Si)N coating showed the lower value (L_{C2} = 36 N), and a sample with Zr-ZrN-(Nb,Zr,Cr,Al)N coating showed the lowest value (L_{C2} = 29 N). Meanwhile, the very failure modes demonstrated by three studied samples show significant differences: the sample with Ti-TiN-(Ti,Cr,Al,Si)N coating showed brittle failure with formation of through cross-cut cracks in combination with minor plastic deformations; the sample with Zr-ZrN-(Nb,Zr,Cr,Al)N coating – brittle failure with formation of delaminations and cracks in inclined plane; and the sample with Zr-ZrN-(Zr,Al,Si)N coating showed sufficient plastic deformation in combination with delaminations between nanolayers;
- the adhesion (molecular) component f_M of the friction coefficient initially increases with the growth of temperature and then begins to decrease sharply with an increase in temperature above 400-450°C;
- an intermediate sublayer introduced into a nano-structured wear-resistant layer produces a visible effect on the failure mode of the coating in case if its thickness is sufficiently higher (9 times) than the average thickness of nanolayers, while if the thickness of sublayer slightly (2 times) differs from thickness of nanolayers, the sublayer does not produce any visible effect on failure of the coating. When a ratio of sublayer thickness to average thickness of nanolayers is 4:1, this sublayer produces insignificant effect on failure of the coating;
- the study of adhesion (molecular) component f_M for tribopairs "alloy S31600–carbide (WC-Co) with coating" within the temperature range of 450-950°C showed that the value of f_M

rises till temperature grows up to 800-850 °C, and with further increase of temperature, f_M starts to decrease;
- samples with ZrN-(Nb,Zr,Cr,Al)N coating showed the lowest value of f_M in the temperature range under the study. The highest f_M was demonstrated by the sample with Ti-TiN-(Ti,Cr,Al,Si)N coating; however, with increase of temperature over 800 °C, f_M shows the most intensive decrease;
- it can be argued that the strength of adhesion bond of coating to substrate L_{C2}, measured at room temperature, produces a greater effect on tool life of a coated tool than adhesion component of COF f_M, measured at high temperatures, at least for the cutting conditions under consideration.

Thus, the qualitative and quantitative results of scratch testing in combination with the data on adhesion (molecular) component of COF f_M for tribopairs of "the material being machined-tool material with coating" make that possible to quite adequately predict a tool life of a coated tool during cutting.

ACKNOWLEDGMENTS

This research was financed by the Ministry of Education and Science of the Russian Federation in the framework of the state order in the sphere of scientific activity (Leading researchers, project 16.9575.2017/6.7).

REFERENCES

[1] B. Navinsek, P. Panjan. Oxidation resistance of PVD Cr, Cr—N and Cr—N—O hard coatings. Surface and Coatings Technology, 59 (1993) 244-248.
[2] I. Milosev, H.-H. Strehblow, B. Navinsek. XPS in the study of high-temperature oxidation of CrN and TiN hard coatings. Surface and Coatings Technology 74-75 (1995) 897-902
[3]L. Rogström, L.J.S. Johnson, M.P. Johansson , M. Ahlgren, L. Hultman, M. Odén. Thermal stability and mechanical properties of arc evaporated ZrN/ZrAlN multilayers. Thin Solid Films 519 (2010) 694–699
[4]I.A. Saladukhin, G. Abadias, V.V. Uglov, S.V. Zlotski, A. Michel, A. Janse van Vuuren. Thermal stability and oxidation resistance of ZrSiNnanocomposite and ZrN/ SiNx multilayered coatings: A comparative study. Surface & Coatings Technology 332 (2017) 428–439
[5] Dobrzanski L A, Lukaszkowicz K, Mikula J, Pakula D. Structure and corrosion resistance of gradient and multilayer coatings [J]. Journal of Achievements in Materials and Manufacturing Engineering, 2006, 18: 75-78.
[6]G. Abadias, L.E. Koutsokeras, A. Siozios, P. Patsalas, Stress, phase stability and oxidation resistance of ternary Ti–Me–N (Me = Zr, Ta) hard coatings, Thin Solid Films 538 (2013) 56
[7] L. Hultman, U, C. Engstrom, M. Oden. Mechanical and thermal stability of TiNrNbNsuperlattice thin films. Surface and Coatings Technology 133-134 2000 227-233
[8] ZhengbingQi, ZhengtaoWu, DongfangZhang, JuanZuo, Zhoucheng Wang. Microstructure, mechanical properties and oxidation behaviors of magnetron sputtered NbNx coatings. Journal of Alloys and Compounds 675 (2016) 22-30
[9] K. Chu, P.W. Shum, Y.G. Shen, Substrate bias effects on mechanical and tribological properties of substitutional solid solution (Ti, Al)N films prepared by reactive magnetron sputtering, Mater. Sci. Eng. B 131 (1–3) (2006) 62–71.

[10] L. Wang, G. Zhang, R.J.K. Wood, S.C. Wang, Q. Xue, Fabrication of CrAlNnanocomposite
films with high hardness and excellent anti-wear performance for gear application, Surf. Coat. Technol. 204 (21–22) (2010) 3517–3524.
[11] B. Yang, L. Chen, K.K. Chang, W. Pan, Y.B. Peng, Y. Du, Y. Liu, Thermal and thermomechanical properties of Ti–Al–N and Cr–Al–N coatings, Int. J. Refract. Met. Hard Mater. 35 (2012) 235–240.
[12] G.S. Fox-Rabinovich, K. Yamamoto, S.C. Veldhuis, A.I. Kovalev, L.S. Shuster, L. Ning, Self-adaptive wear behavior of nano-multilayered TiAlCrN/WN coatings under severe machining conditions, Surf. Coat. Technol. 201 (2006) 1852–1860.
[13] G.S. Fox-Rabinovich, K. Yamomoto, S.C. Veldhuis, A.I. Kovalev, G.K. Dosbaeva, Tribological adaptability of TiAlCrN PVD coatings under high performance dry machining conditions, Surf. Coat. Technol. 200 (2005) 1804–1813.
[14] M. Danek, F. Fernandes, A. Cavaleiro, T. Polcar, Influence of Cr additions on the structure and oxidation resistance of multilayered TiAlCrN films, Surf. Coat. Technol. 313 (2017) 158–167.
[15] P. Ou, J. Wang, S. Shang, L. Chen, Y. Du, Z.-K. Liu, F. Zheng, A first-principles study of structure, elasticity and thermal decomposition of $Ti_{1-x}TM_xN$ alloys (TM = Y, Zr, Nb, Hf, and Ta), Surf. Coat. Technol. 264 (2015) 41-48.
[16] H. Kindlund, D.G. Sangiovanni, L. Martinez-de-Olcoz, J. Lu, J. Jensen, J. Birch, I. Petrov, J.E. Greene, V. Chirita, L. Hultman, Toughness enhancement in hard ceramic thin films by alloy design, Appl. Phys. Lett. Mater 1 (2013) 042104.
[17] D.G. Sangiovanni, V. Chirita, L. Hultman, Toughness enhancement in TiAlN based quaternary alloys, Thin Solid Films 520 (2012) 4080–4088
[18] R. Forsén, M.P. Johansson, M. Odén, N. Ghafoor, Effects of Ti alloying of AlCrN coatings on thermal stability and oxidation resistance, Thin Solid Films, 534 (2013) 394-402.
[19] Y.X. Xu, H. Riedl, D. Holec, L. Chen, Y. Du, P.H. Mayrhofer, Thermal stability and oxidation resistance of sputtered TiAlCrN hard coatings, Surface and Coatings Technology, 324 (2017) 48-56.
[20] Marian Mikula, DusanPlasienka, Davide G. Sangiovanni , Martin Sahul,TomasRoch , Martin Truchlý, MarosGregor, LubomírCaplovic, Andrej Plecenik, Peter Kús. Toughness enhancement in highly NbN-alloyed Ti-Al-N hard coatings.ActaMaterialia 121 (2016) 59-67
[21] Y.H. Chen, J.J. Roa, C.H. Yu, M.P. Johansson-Jöesaar, J.M. Andersson, M.J. Anglada, M. Odén, L. Rogström. Enhanced thermal stability and fracture toughness of TiAlN coatings by Cr, Nb and V-alloying. Surface & Coatings Technology. Accepted Manuscript. doi:10.1016/j.surfcoat.2018.02.059
[22] Y. Dong, Y. Liu, J. Dai, G. Li, SuperhardNb–Si–N composite films synthesized by reactive magnetron sputtering, Appl. Surf. Sci. 252 (2006) 5215–5219
[23] F. Ge, T. Shao, C.Jia, P. Li, F. Huang. Tribological behaviors of a magnetron sputtered CrSiN coating under ambient air and wet environments. Surface & Coatings Technology 332 (2017) 304–311
[24] F. Gaoa, G. Li , Y. Xia. Influence of hysteresis effect on properties of reactively sputtered TiAlSiN films. Applied Surface Science 431 (2018) 160–164
[25] D. B. Lee, S. K. Kim. Oxidation of ZrAlSiNnano-multilayered thin films between 400 and 600 °C. Surface & Coatings Technology 259 (2014) 68–70
[26] Chun-Chi Chang, Jenq-Gong Duh. Duplex coating technique to improve the adhesion and tribological properties of CrAlSiNnanocomposite coating. Surface & Coatings Technology 326 (2017) 375–381
[27] V.V. Uglov, G. Abadias, S.V. Zlotski, I.A. Saladukhin, V.A. Skuratov, S.S. Leshkevich, S. Petrovich. Thermal stability of nanostructured TiZrSiN thin films subjected

to helium ion irradiation. Nuclear Instruments and Methods in Physics Research B 354 (2015) 264–268
[28] D.K. Lee, D.S. Kang, J.H. Suh, C.G. Park, K.H. Kim, Synthesis and mechanical evaluation
of quaternary Ti–Cr–Si–N coatings deposited by a hybrid method of arc ion plating and sputtering techniques, Surf. Coat. Technol. 200 (2005) 1489–1494.
[29]Y.H. Yoo, J.H. Hong, J.G. Kim, H.Y. Lee, J.G. Han, Effect of Si addition to CrN coatings on the corrosion resistance of CrN/stainless steel coating/substrate system in a deaerated 3.5 wt.% NaCl solution, Surf. Coat. Technol. 201 (2007) 9518–9523.
[30] C.M. Koller, R. Hollerweger, C. Sabitzer, R. Rachbauer, S. Kolozsvári, J. Paulitsch, P.H. Mayrhofer, Thermal stability and oxidation resistance of arc evaporated TiAlN, TaAlN, TiAlTaN, and TiAlN/TaAlN coatings, Surf. Coat.Technol. 259 (2014) 599.
[31] Li Chen, Yu X. Xu, Li J. Zhang. Influence of TiN and ZrN insertion layers on the microstructure, mechanical and thermal properties of Cr–Al–N coatings. Surface & Coatings Technology 285 (2016) 146–152
[32]A. A. Vereschaka, Ju. I. Bublikov, N. N. Sitnikov, G. V. Oganyan and C. S. Sotova. Influence of nanolayer thickness on the performance properties of multilayer composite nano-structured modified coatings for metal-cutting tools. International Journal of Advanced Manufacturing Technology.(2018) 95:2625–2640
[33]A.S. Vereschaka, A.A. Vereschaka, D.V. Sladkov, A. Yu. Aksenenko and N.N. Sitnikov. Control of structure and properties of nanostructured multilayer composite coatings applied to cutting tools as a way to improve efficiency of technological cutting operation. Journal of Nano Research. Vol. 37 (2016) pp 51-57
[34]A. A. Vereschaka, A. S. Vereschaka, Ju. I. Bublikov, A. Y. Aksenenko, N. N. Sitnikov. Study of properties of nanostructured multilayer composite coatings of Ti-TiN-(TiCrAl)N and Zr-ZrN-(ZrNbCrAl)N. Journal of Nano Research. Vol. 40 (2016) pp 90-98
[35]A.Vereschaka, E. Kataeva , N. Sitnikov, A. Aksenenko, G. Oganyan and C. Sotova. Influence of Thickness of Multilayered Nano-Structured Coatings Ti-TiN-(TiCrAl)N and Zr-ZrN-(ZrCrNbAl)N on Tool Life of Metal Cutting Tools at Various Cutting Speeds. Coatings 2018, 8, 42
[36] A.A. Vereschaka, M.A. Volosova, A.D. Batako, A.S. Vereshchaka, B.Y. Mokritskii, Development of wear-resistant coatings compounds for high-speed steel tool using a combined cathodic vacuum arc deposition, Int. J. Adv. Manuf. Tech. 84 (2016)1471–1482.
[37] A.A. Vereschaka, A.S. Vereschaka, A.D. Batako, O.K. Hojaev, B.Y. Mokritskii, Development and research of nanostructured multilayer composite coatings for tungsten-free carbides with extended area of technological applications, Int. J. Adv. Manuf. Tech. 87 (2016) 3449–3457.
[38] A.A. Vereschaka, S.N. Grigoriev. Study of cracking mechanisms in multi-layered composite nano-structured coatings. Wear. 378-379 (2017) 43–57.
[39] Alexey A. Vereschaka, Sergey N. Grigoriev, Nikolay N. Sitnikov, Gaik V. Oganyan and Andre Batako. Working efficiency of cutting tools with multilayer nano-structured Ti-TiCN-(Ti,Al)CN and Ti-TiCN-(Ti,Al,Cr)CN coatings: Analysis of cutting properties, wear mechanism and diffusion processes. Surface and Coatings Technology 332 (2017) 198–213.
[40] A.O. Volkhonskii, A.A. Vereshchaka, I.V. Blinkov, A.S. Vereshchaka, A.D. Batako, Filtered cathodic vacuum Arc deposition of nano-layered composite coatings for machining hard-to-cut materials, Int. J. Adv. Manuf. Tech. 84 (2016) 1647–1660.

[41] A.A. Vereschaka, S.N. Grigoriev, A.S. Vereschaka, A.Y. Popov, A.D. Batako, Nano-scale multilayered composite coatings for cutting tools operating under heavy cutting conditions, Procedia CIRP. 14 (2014) 239–244. DOI:10.1016/j.procir.2014.03.070
[42] A.A. Vereschaka, S.N. Grigoriev, N.N. Sitnikov and Andre Batako.Delamination and longitudinal cracking in multi-layered composite nano-structured coatings and their influence on cutting tool life.*Wear*. 390–391 (2017) 209–219
[43]B.D.Beake ,G.S.Fox-Rabinovich. Progress in high temperature nanomechanical testing of coatings for optimizing their performance in high speed machining. Surface & Coatings Technology 255,2014,p.102–111
[44]G.S.Fox-Rabinovich, B.D.Beake, S.C.Veldhuis, J.L.Endrino, R.Parkinson, L.S.Shuster,M.S.Migranov, Effect of mechanical properties measured at room and elevated temperatures on the wear resistance of cutting tools with TiAlN and AlCrN coatings. Surface & Coatings Technology.200, 2006,p.5738-42.
[45]J.Nohava, P.Dessarzin, P. Karvankova, M.Morstein. Characterization of tribological behavior and wear mechanisms of novel oxynitride PVD coatings designed for applications at high temperatures. Tribology International 81 ,2015, p. 231–239
[46]M. Bao, X. Xu, H. Zhang, X. Liu, L. Tian, Z. Zeng, Y. Song. Tribological behavior at elevated temperature of multilayer TiCN/TiC/TiN hard coatings produced by chemical vapor deposition.ThinSolidFilms520 ,2011, p. 833–836
[47]L.Sh. Shuster. Adhesive interaction of the cutting tool with the material being processed. Mashinostroenije, Moscow,1988, 96 p.
[48]L.Sh. Shuster et al. Device for investigating adhesion interaction. Patent of Russia 34249 26/03/2003.
[49] L.C. Feldman, J.W. Mayer. Fundamentals of surface and thin film analysis.North-Holland. New York. 1986
[50] Y.H. Chen, L. Rogström, J.J. Roa, J.Q. Zhu, I. C. Schramm, L.J.S. Johnson, N.Schell, F. Mücklich, M.J. Anglada and M. Odén. Thermal and mechanical stability of wurtzite-ZrAlN/cubic-TiN and wurtziteZrAlN/cubic-ZrN multilayers. Surface and Coatings Technology. Vol. 324, 2017, P. 328-337
[51] H. Lind, R. Forsen, B. Alling, N. Ghafoor, F. Tasnadi, M.P. Johansson, I.A. Abrikosov, M. Oden, Appl. Phys. Lett. 99 (2011) 091903.
[52] L. Rogstrom, M. Ahlgren, N. Ghafoor, and M. Oden.Auto-organizing in ZrAlN/ZrAlTiN/TiN multilayers. Thin Solid Films 520 (2012) 6451–6454
[53] S.H. Sheng, R.F. Zhang, S. Veprek. Phase stabilities and thermal decomposition in the $Zr_{1-x}Al_xN$ system studied by ab initio calculation and thermodynamic modeling. ActaMaterialia 56 (2008) 968–976
[54] A. Hoerling, J. Sjölén, H. Willmann, T. Larsson, M. Odén, L. Hultman. Thermal stability, microstructure and mechanical properties of Ti1 − xZrxN thin films. Thin Solid Films 516 (2008) 6421–6431
[55] M. Mikula, D. Plasienka, D. G. Sangiovanni , M.Sahul,T. Roch , M.Truchlý, M. Gregor, L. Caplovic, A.Plecenik, P.Kús. Toughness enhancement in highly NbN-alloyed Ti-Al-N hard coatings. Acta Materialia 121 (2016) 59-67
[56]H. C. Barshilia, A. Jain, K.S. Rajam.Structure, hardness and thermal stability of nanolayeredTiN/CrN multilayer coatings. Vacuum 72 (2004) 241–248
[57] F. Maury, D. Duminica and F.Seconq.Novel MOCVD for the low temperature of chromium nitrides phases. CVD XV: Proceedings of the Fifteenth International Symposium on Chemical Vapor Deposition , The Electrochemical Society, 2000. 260-266 pp]

[58] ASTM C1624-05(2010), Standard Test Method for Adhesion Strength and Mechanical Failure Modes of Ceramic Coatings by Quantitative Single Point Scratch Testing, ASTM International, West Conshohocken, PA, 2010